Precambrian Research 305 (2018) 247–267

Contents lists available at ScienceDirect

Precambrian Research

journal homepage: www.elsevier.com/locate/precamres

Pluton construction and deformation in the Sveconorwegian crust of SW Norway: Magnetic fabric and U-Pb geochronology of the Kleivan and Sjelset granitic complexes

Olivier Bolle[a,*,1], Hervé Diot[b,c], Jacqueline Vander Auwera[a], Aliou Dembele[a], Jasmine Schittekat[a,d], Simo Spassov[e], Maria Ovtcharova[f], Urs Schaltegger[f]

[a] Département de Géologie, Université de Liège, Allée du Six Août 12, 4000 Sart Tilman, Belgium
[b] UMR-CNRS 6112, Laboratoire de Planétologie et Géodynamique, Université de Nantes, Rue de la Houssinière 2, 44322 Nantes Cedex 3, France
[c] Faculté de Sciences et Technologie, Université de La Rochelle, Avenue M. Crépeau, 17402 La Rochelle Cedex 1, France
[d] SGS Belgium NV, Parc Créalys, Rue Phocas Lejeune 4, 5032 Gembloux, Belgium
[e] Centre de Physique du Globe, Institut Royal Météorologique, Rue du Centre de Physique 1, 5670 Dourbes, Belgium
[f] Département des Sciences de la Terre, Université de Genève, Rue des Maraîchers 13, 1205 Genève, Switzerland

ARTICLE INFO

Keywords:
Anisotropy of magnetic susceptibility
Zircon geochronology
CA-ID-TIMS U-Th-Pb dating
Synfolding
Granite emplacement
Sveconorwegian orogeny

ABSTRACT

The Kleivan and Sjelset granitic complexes are two composite plutons, containing both orthopyroxene and biotite (± hornblende) facies, emplaced in the Sveconorwegian (Grenvillian) high-grade basement of SW Norway. A structural study of these two plutons, based on the anisotropy of magnetic susceptibility (AMS) technique and combined with high-precision U-Th-Pb zircon dating, is presented here. Geochronological data demonstrate a rapid emplacement of successive magmatic pulses in the Kleivan complex (from 936.94 ± 0.42 Ma to 935.62 ± 0.67 Ma) and, on the contrary, a non-negligible rest period (~3.2 Ma) in the construction of the Sjelset complex that was formed by two pulses emplaced, respectively, at 935.67 ± 0.37 Ma and 932.43 ± 0.75 Ma. Locally discordant magnetic fabrics in the latter pluton confirm this rather protracted construction time. Thermomagnetic and hysteresis measurements supporting the AMS data indicate a magnetic mineralogy dominated by a multidomain, Ti-poor titanomagnetite, except in samples having a very low magnetic susceptibility. The susceptibility magnitudes, paramagnetic to ferromagnetic in agreement with the rock magnetic data, rely on the petrographic rock-types and on the alteration degree. Image analysis confirms that the magnetic fabric is usually coaxial with the shape fabric in both complexes, supporting the use of AMS as a proxy for the petrofabric orientation. Combined with micro- and macrostructural data, the magnetic fabric demonstrates that the Kleivan and Sjelset granitic complexes have their internal fabrics largely dominated by tectonic strain. Models of synfolding emplacement coeval with the last stage of Sveconorwegian contraction recorded in the area are proposed for the two plutons.

1. Introduction

During the 1980–1990s, in the lively debate about ascent and emplacement of granitic magmas into the Earth's crust, a major step was taken when it was recognized that both processes are commonly controlled by active major faults or shear zones, regardless of the tectonic setting (Hutton, 1988; D'Lemos et al., 1992; among others). At the same time, increasing fabric studies of granitic plutons and batholiths using the anisotropy of magnetic susceptibility (AMS) technique led to another major conclusion (Bouchez, 2000): despite their massive aspect, granites *s.l.* (granitoids) commonly display homogeneous fabrics that mimic the tectonic pattern of the wall rocks, leading to the idea that almost all granitoids are syntectonic. Fabric in granitoids is therefore a first-rate witness of regional tectonics, especially, but not exclusively, in contractional or transpressive contexts (Bouchez et al., 1990; Benn et al., 1997; Gleizes et al., 1998; Román-Berdiel et al., 2004; Henry et al., 2009; among others). It was also found that the ability of granitic plutons to record contemporaneous tectonic strain during their growth is variable (Benn et al., 1998; Paterson et al., 1998; de Saint Blanquat et al., 2011): rapidly cooled syntectonic plutons, *i.e.* bodies of small size and/or emplaced at shallow depth, display fabrics dominated by syn- to post-emplacement internal processes (magmatic flow or magma

* Corresponding author.
E-mail address: olivier.bolle@ulg.ac.be (O. Bolle).
[1] Research Associate from the F.N.R.S., Belgium.

https://doi.org/10.1016/j.precamres.2017.12.012
Received 20 July 2017; Received in revised form 28 November 2017; Accepted 4 December 2017
Available online 05 December 2017
0301-9268/

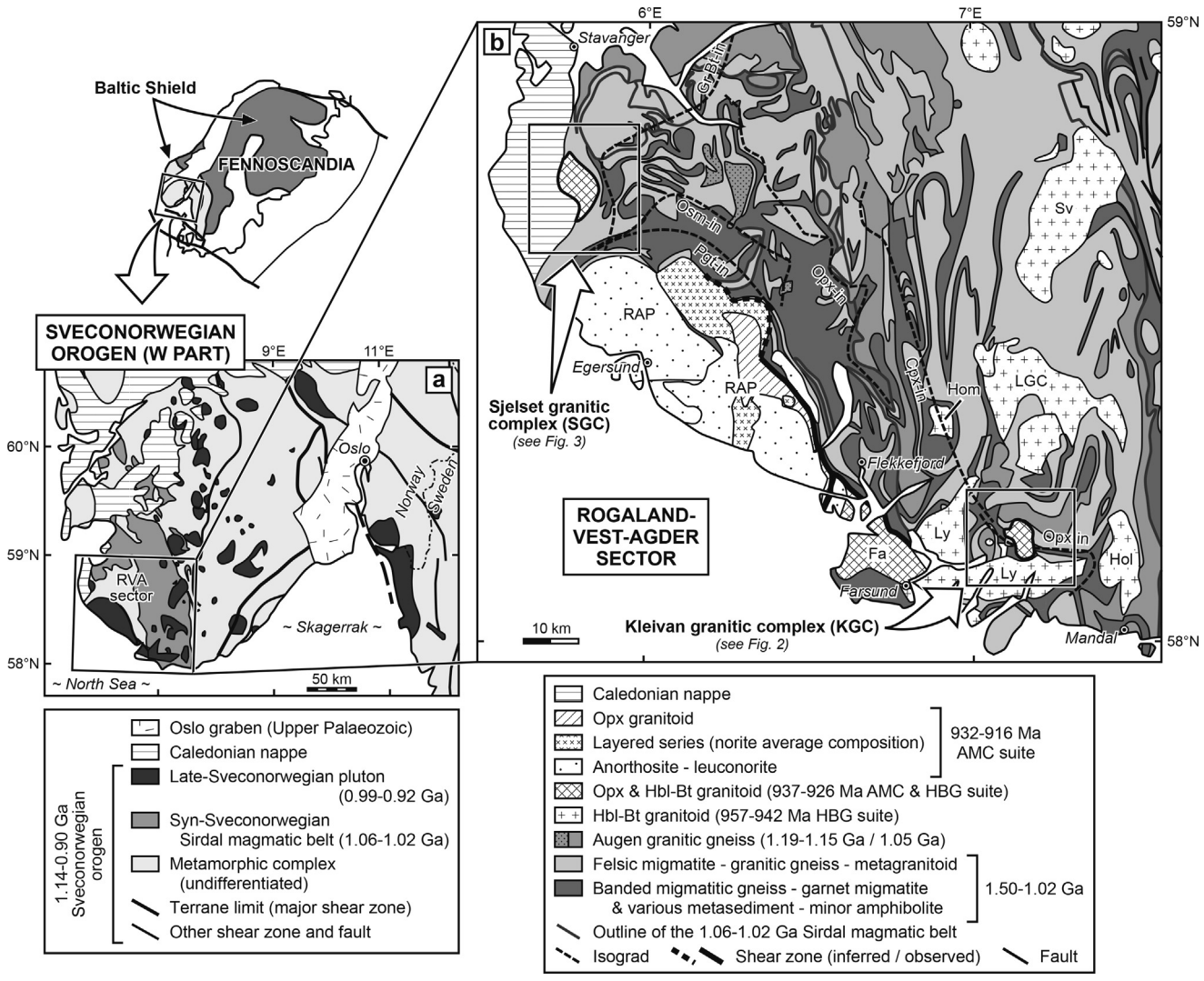

Fig. 1. (a) Sketch map of the western portion of the Sveconorwegian orogen (simplified from Bingen et al., 2005; Sirdal magmatic belt modified from Slagstad et al., 2013 and Coint et al., 2015, with speculative outlines in the Caledonides area; inset map of Fennoscandia simplified after Bogdanova et al., 2008). RVA sector, Rogaland-Vest-Agder sector. (b) Geological map of the Rogaland-Vest-Agder sector (after Sigmond et al., 1984 and Coint et al., 2015; boundaries for the Rogaland anorthosite province and the Farsund intrusion from Marker et al., 2003 and references in Bolle et al., 2010; isograds from Petersen, 1980; Tobi et al., 1985; Bingen et al., 1996; shear zone along the eastern margins of the Rogaland anorthosite province and Farsund intrusion (Farsund-RAP shear zone) from Bolle et al., 2010; faults in the east of the sector from Falkum, 1982). Acronyms, roughly from west to east: Gr Bt-in, Pig-, Osm-, Opx- and Cpx-in, green-biotite-, (inverted) pigeonite-, osumilite-, orthopyroxene- and clinopyroxene-in isograds; RAP, Rogaland anorthosite province; Fa, Farsund intrusion; Ly, Lyngdal granodiorite; Hom, Homme granite; LGC, Lygne granitic complex; Hol, Holum granite; Sv, Svöfjell granite. Ages quoted in the legend are U-Pb dates published or compiled by Bingen et al. (2005, 2008b), Vander Auwera et al. (2011, 2014), Slagstad et al. (2013) and Coint et al. (2015), to which U-Pb emplacement ages of the KGC and SGC from the present study have been added.

chamber dynamics) and syntectonic bodies of various sizes, the largest ones particularly, may display remnants of such igneous processes.

Here, we present a magnetic fabric (AMS) study of the Kleivan and Sjelset granitic complexes (KGC and SGC), supported by thermomagnetic and hysteresis measurements, as well as image analysis, and combined with high-precision U-Th-Pb zircon dating. The KGC and SGC are two early Neoproterozoic (Tonian) granitoids from the Sveconorwegian (= Grenvillian) high-grade basement of SW Norway (Fig. 1a). The Sveconorwegian crust in the area is characterized by a complex tectono-metamorphic history (*e.g.* Bingen et al., 2006, 2008a,b) whose late evolution was marked by the emplacement of mostly granitic plutons, as represented by the KGC and SGC previously studied on a geochemical point of view by Petersen (1980), Maijer et al. (1994), and Jacamon and Larsen (2009). Most late-Sveconorwegian granitoids have been considered as post-tectonic intrusions (Starmer, 1993; Falkum, 1998), despite basic observations such as the common elongation of plutons parallel to the regional tectonic framework suggesting syn- to post-emplacement tectonic deformation. In other words, these granitoids, including the KGC and SGC are potential markers of the late-Sveconorwegian tectonics, which has been confirmed by previous AMS studies (Bolle et al., 2003, 2010).

The KGC and SGC are made of contrasted rock facies, interpreted as either contemporaneous magmatic batches (KGC; Petersen and Pedersen, 1978; Petersen, 1980) or pulses separated by a long time gap (SGC; Maijer et al., 1994; Coint et al., 2015). Hence, the first goal of the present integrated study is to date the KGC and SGC, in order to determine their construction time. The study also aims at characterizing the geometrical and temporal relationships of the two complexes with other late-Sveconorwegian plutons and regional structures formed in the waning stage of the Sveconorwegian orogeny. The present paper contributes to the improved knowledge of emplacement mechanisms of granitoids in high-grade terranes.

2. Geological setting

2.1. The Sveconorwegian orogen

The 1.14–0.90 Ga Sveconorwegian belt (Fig. 1a) forms the SW and youngest portion of the Baltic Shield, *i.e.* the exposed part of Fennoscandia, a segment of the Baltica paleocontinent (Bogdanova et al., 2008). This orogen is divided into N-S to NW-SE-trending terranes made of Paleo- to Mesoproterozoic crust and separated by major shear-zones. Its central part is cut obliquely by the late Carboniferous to Permian Oslo graben and its western border is largely covered by Caledonian nappes. Classically, the Sveconorwegian orogen is regarded as one of several Grenvillian belts (*e.g.* Li et al., 2008) and pictured as a polyphase imbrication of crust resulting from oblique collision and convergence between the SW margin of Baltica and, possibly, Amazonia (Bingen et al., 2005, 2008b). This model has been recently challenged by Slagstad et al. (2013) who suggested that the Sveconorwegian belt would be a non-collisional accretionary orogen in which the subduction did not lead to collision. One of their argument, relayed by Coint et al. (2015), is to propose that a large belt of calc-alkaline granitoids (the Sirdal magmatic belt) was emplaced at 1.06–1.02 Ga in the westernmost part of the orogen, thus suggesting an Andean arc setting in the area at that time.

Biotite ± hornblende granitoids are abundant in the Sveconorwegian orogen (Andersen et al., 2001; Eliasson et al., 2003; Vander Auwera et al., 2003, 2008). They are concentrated into two roughly N-S-trending belts geographically associated with large-scale shear zones (Fig. 1a). Anorthosite to charnockite plutons crop out to the SW of the western belt of granitoids (Duchesne et al., 1985; Duchesne, 2001), forming the Rogaland anorthosite province (RAP; Fig. 1a, b). In the conventional, collisional model admitted for the Sveconorwegian orogen, the biotite ± hornblende granitoids and the RAP, that were emplaced in the interval 0.99–0.92 Ga, are considered as the product of post-collisional magmatism and ascribed to a phase of gravitational collapse of the orogenic belt, following collision-induced crustal thickening (Bingen et al., 2006, 2008b). In the challenging, non-collisional accretionary model of Slagstad et al. (2013), these plutons are supposed to record a return to an extensional subduction regime, after a period of flattening of the subducting slab. We will simply refer here to late-Sveconorwegian plutonism.

2.2. The Rogaland-Vest-Agder sector

The Rogaland-Vest-Agder (RVA) sector is the southwesternmost domain of the Sveconorwegian belt (Fig. 1a, b). It consists of a high-grade gneiss complex intruded by several late-Sveconorwegian plutons, including the KGC and SGC.

A subdivision between three main lithological units, namely “banded gneiss”, “granitic gneiss” and “augen gneiss”, is traditionally referred to in the RVA high-grade gneiss complex (Fig. 1b; Falkum, 1982, 1998; Bingen and van Breemen, 1998). The banded gneisses are variably migmatitic and correspond, at least partly, to metasediments. The granitic gneisses and augen gneisses are derived from granitoids, most augen gneiss units belonging to the syn-Sveconorwegian (1.05 Ga) calc-alkaline Feda suite. However, Coint et al. (2015) consider that most rocks mapped as granitic gneisses and banded gneisses in the east and north of the RVA sector are, respectively, metagranitoids and associated rafts of mafic xenoliths. These “granitic gneisses”, together with the Feda suite are the main components of the 1.06–1.02 Ga Sirdal magmatic belt.

The late-Sveconorwegian plutonism in the RVA sector is represented by two petrographically, chemically and geographically distinct suites of A-type affinity (Fig. 1b; Vander Auwera et al., 2003): a hornblende-biotite granitoid (HBG) suite described all over Southern Norway and an orthopyroxene or anorthosite-mangerite-charnockite (AMC) suite restricted to the RVA sector. The plutons defining the HBG suite belong to the western belt of late-Sveconorwegian granitoids. The AMC suite is defined by the RAP. The HBG plutons are dated at 957–942 Ma in the RVA sector and the RAP was built in a short period of time at 932–916 Ma (U-Pb ages; Schärer et al., 1996; Vander Auwera et al., 2011; and references therein). Three composite late-Sveconorwegian plutons, containing both orthopyroxene and hornblende-biotite granitoids are found in the surroundings of the RAP, namely, from W to E, the SGC, the Farsund intrusion and the KGC (Fig. 1b). The orthopyroxene and hornblende-biotite granitoids that constitute the Farsund intrusion, the most voluminous composite pluton, crystallized from coeval magma batches with, respectively, AMC and HBG signatures, and U-Pb ages of 931 ± 2 Ma and 926 ± 4 Ma (Vander Auwera et al., 2014).

Petrological data indicate a sequence of three Sveconorwegian metamorphic phases in the RVA gneiss complex (Maijer, 1987), dated by U-Pb, Th-Pb and Re-Os geochronology (Bingen et al., 2008a; Drüppel et al., 2013; and references therein both works): M1, a medium-*P* prograde metamorphic stage recording crustal thickening (1.035–0.97 Ga), followed by regional decompression (0.97–0.955 Ga); M2, a stage of low-*P* contact metamorphism induced by the emplacement of the RAP (0.93–0.92 Ga); M3, a retrograde stage related to post-M2 isobaric cooling. These three superimposed metamorphic phases resulted in a high-grade metamorphism, increasing westwards from upper-amphibolite to granulite facies, as reflected by a sequence of four isograds, namely, from NE to SW (Fig. 1b; Tobi et al., 1985; Bingen et al., 1996): clinopyroxene-, orthopyroxene-, osumilite- and (inverted) pigeonite-in isograds. The *P-T* conditions of M1, M2 and M3, as well as their genetic relationships with the Sveconorwegian isograds are still under debate (*e.g.* Drüppel et al., 2013). An incipient, Caledonian retrograde metamorphism has also been documented (M4; Maijer, 1987). It is a polyphase metamorphism, resulting from the overlap of two successive phases: M4a, a burial metamorphism of lower-Paleozoic age, mainly in prehnite-pumpellyite facies (Sauter et al., 1983), and M4b, largely in lower-greenschist facies conditions, related to the Caledonian thrusting, hence restricted to the vicinity of the Caledonides (Verschure et al., 1980). The M4b phase is responsible for a green-biotite-in isograd in the gneiss complex to the east of the Caledonian front (Fig. 1b).

Structural studies conducted in different areas of the RVA sector identified several successive phases of deformation in the high-grade gneisses, revealed by refolded folds. The most recent study, taken here as a reference, is the one of Falkum (1998) that describes six folding phases (F1 to F6) to the SE of the RAP. The youngest phase of deformation (F6) produced mesoscopic to large-scale (kilometric), dominantly open to gentle folds, with E-W axes and steep axial planes. Most former superimposed folds developed along *ca.* N-S-trending axes, giving rise to the dominantly N-S-trending structural pattern of the gneisses (Fig. 1b). The last generation of *ca.* N-S folds (F5) is characterized by tight to open folds, with N-S- to NE-SW-striking axes and steep axial planes. Most late-Sveconorwegian plutons in the RVA sector, called “post-tectonic” or “post-kinematic”, apparently escaped regional folding and are supposed to post-date F6, whereas some of them, called “late-tectonic” or “late-kinematic”, were obviously affected by F5 (and locally F6) and are therefore considered to have been emplaced before F5-F6 (Starmer, 1993; Falkum, 1998).

Sveconorwegian faults and shear zones occur in the RVA sector (Fig. 1b). In particular, a steeply-dipping shear zone, characterized by an oblique slip of undefined sense straddles the eastern margins of the RAP and Farsund intrusion. This high-strain zone, called the Farsund-RAP shear zone, is a major structure that would have controlled the ascent and emplacement of both the RAP and the Farsund intrusion (Bolle et al., 2010).

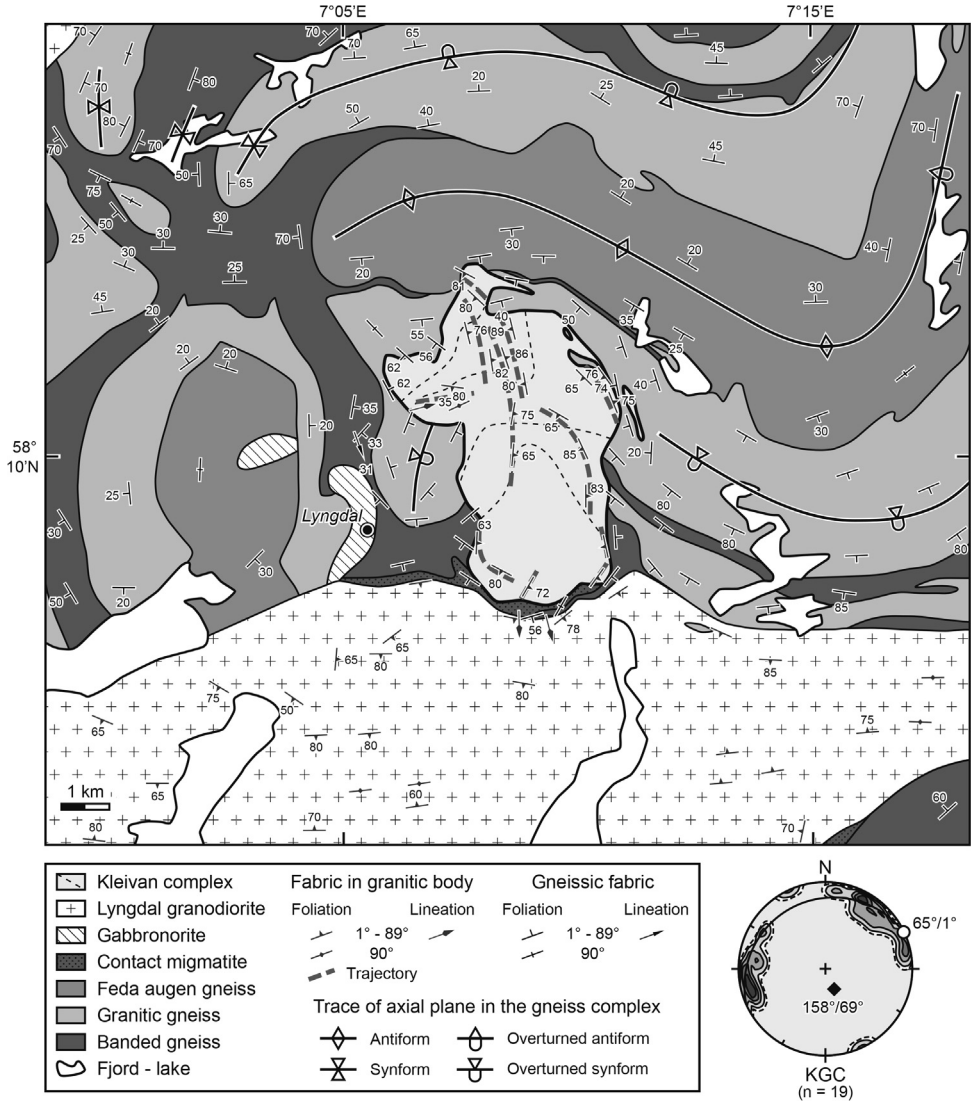

Fig. 2. Geological map of the Kleivan granitic complex (KGC) and its surroundings. Simplified from Petersen (1977, 1980) and Falkum (1982), with additional structural data from Petersen (1973), and Falkum and Petersen (1974). Most foliation and lineation measurements in the pluton and some of them near the margins are from this study. Internal divisions of the complex: see text and Fig. 4a. The contoured equal-area projection shows the distribution of foliation poles in the pluton (lower hemisphere; contours at 1–2–4–6–8%; white dot: weighted average; great circle and black diamond: best fit girdle and its pole). Note: according to Coint et al. (2015), units of granitic gneiss and banded gneiss in the area are, respectively, metagranitoids and associated rafts of mafic enclaves belonging, together with the Feda augen gneiss, to the Sirdal magmatic belt.

3. The country rocks of the Kleivan and Sjelset granitic complexes

3.1. Description

The country rocks of the KGC consist of alternating units of banded gneiss, granitic gneiss and Feda augen gneiss (Fig. 2), all belonging to the Sirdal magmatic belt according to Coint et al. (2015). Their metamorphic grade increases southwards, from upper-amphibolite to granulite facies (Fig. 1b). The lithology of the SGC wall rocks is more variable (Fig. 3): granitic gneiss, banded gneiss, various migmatitic gneisses (including garnet paragneiss), paragneisses (mainly quartz-diopside gneiss) belonging to the so-called Faurefjell metasediment formation and metagranitoids whose largest body, to the NE, pertains to the Sirdal magmatic belt. These rocks belong to the granulite-facies domain (Fig. 1b). They have been affected, as the SGC itself, by the Caledonian retrograde metamorphism, especially the M4b phase due to the proximity of Caledonian nappes that cover the SGC and the adjacent gneisses to the west (Fig. 3). HBG plutons crop out in the vicinity of the KGC (Figs. 1b, 2): two small gabbronorite bodies (Vander Auwera et al., 2003) to the west and the 950 ± 5 Ma Lyngdal granodiorite (Bogaerts et al., 2003) to the south, the latter being separated from the KGC by a thin septum of banded gneiss and "contact migmatite" (a brecciated migmatite made of a granitic material containing numerous angular mafic fragments; Falkum and Petersen, 1974; Petersen, 1977).

The main mesoscopic structural elements in the country rocks of both granitic complexes are planar features, mostly a compositional layering and a usually concordant schistosity, collectively here referred to a gneissic foliation. Mineral and stretching lineations occur, but are not always easy to measure in the field. In the country rocks of the KGC, Petersen (1973) demonstrated the existence of at least three interfering generations of folds. The youngest and largest interference pattern results from the refolding of isoclinal to open, upright to moderately-inclined synforms and antiforms with dominantly gently-plunging axes (see the trace of their axial planes in Fig. 2), by *ca.* N-S-trending, steeply-inclined folds with axes of variable plunges (probably equivalent to F5 folds; not drawn in Fig. 2 since their detailed geometry was not given by Petersen, 1973). In the surroundings of the SGC, Michot (1960) recognized two phases of isoclinal folding and a third generation of folds characterized by steeply-dipping axial planes and E-W axes (probably equivalent to F6 folds). The second deformation phase of Michot (1960) would have participated to large thrust sheets (Fig. 3) that are unknown outside the area he mapped. Variations of the foliation orientation in the SGC wall rocks result at most places from the intrusion of plutonic rocks rather than from regional deformation, which distorts the N-S-trending structural pattern of the gneisses (*e.g.* to the north of the RAP; Figs. 1b, 3).

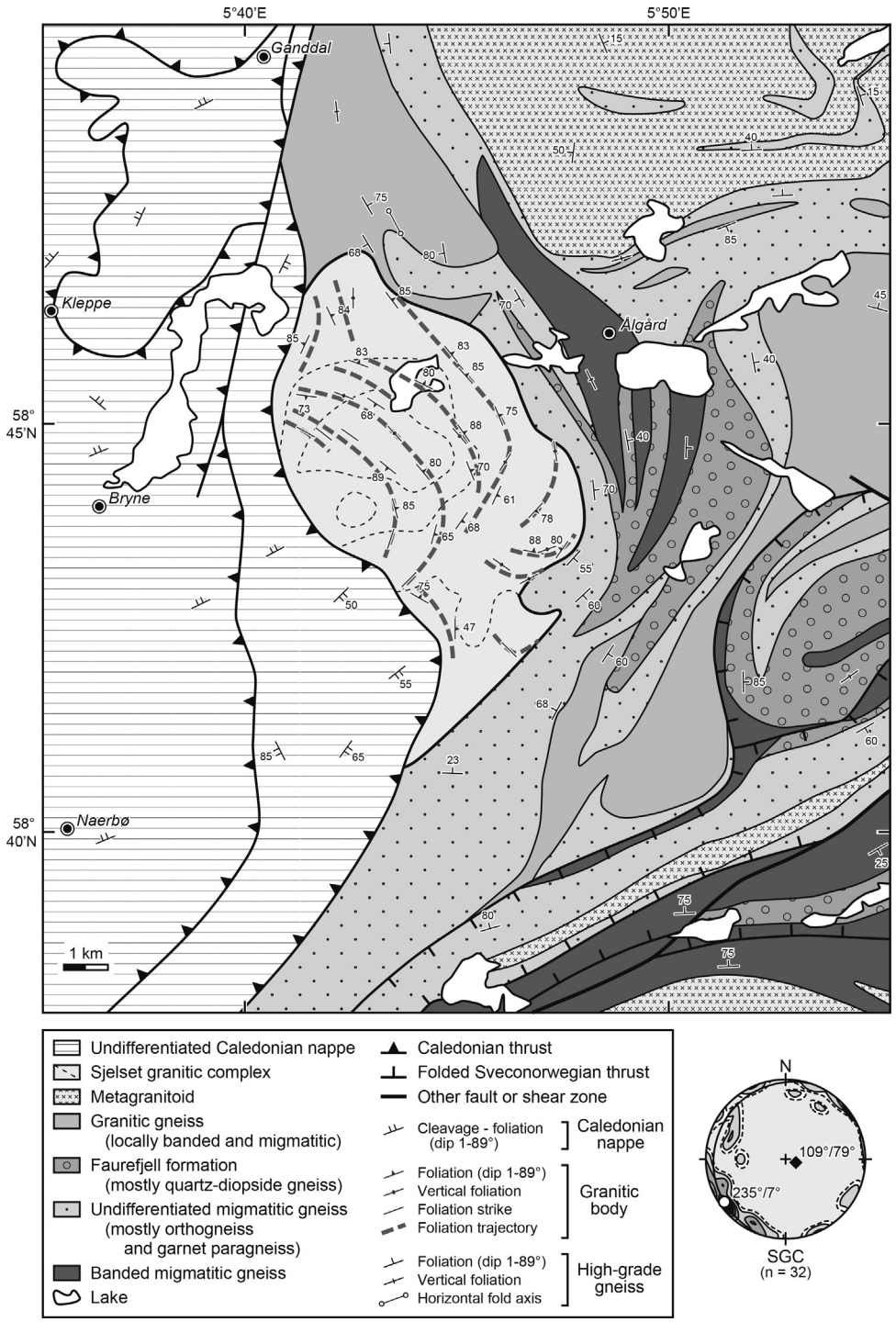

Fig. 3. Geological map of the Sjelset granitic complex (SGC) and its surroundings. Simplified from Jorde et al. (1995) and, for the NE corner of the map, Coint et al. (2015), with additional information from Marker et al. (2003). All foliation measurements in the pluton and some of them near the margins are from this study. Internal divisions of the complex: see text and Fig. 4b. The contoured equal-area projection shows the distribution of foliation poles in the pluton (lower hemisphere; contours at 1–2–4–6–8–10%; white dot: weighted average; great circle and black diamond: best fit girdle and its pole).

3.2. Relationships with the two plutons

The KGC and SGC form, in map view, N-S-elongated bodies (~20 km^2 and ~43 km^2, respectively; Figs. 2, 3). The elongate shape is obvious for the KGC and deduced for the SGC from its outline and from the aeromagnetic map of the area that precludes, according to Bingen (personal communication, 2017), any important extension under the Caledonian nappes. These elongate bodies are orientated parallel to the N-S-striking pattern of the high-grade gneiss complex (Fig. 1b). However, at the local scale, both complexes are clearly discordant against the gneisses, except where their emplacement has transposed the latter, as seen at the northern and NE contacts of the KGC where granitic material forms a small outlier parallel to the gneissic foliation (Fig. 2) and at the eastern boundary of the SGC (Fig. 3). According to Petersen (1980), the KGC also affects the neighbouring gneisses near its southern margins where a well-defined lineation is locally developed in the wall rocks, at the intersection between the gneissic foliation and a cleavage plane parallel to the contact.

4. Petrology and field structures of the Kleivan and Sjelset granitic complexes

The KGC exhibits a conspicuous N-S variation of its composition: a charnockite (orthopyroxene granite, referred to as Opx-facies) is found

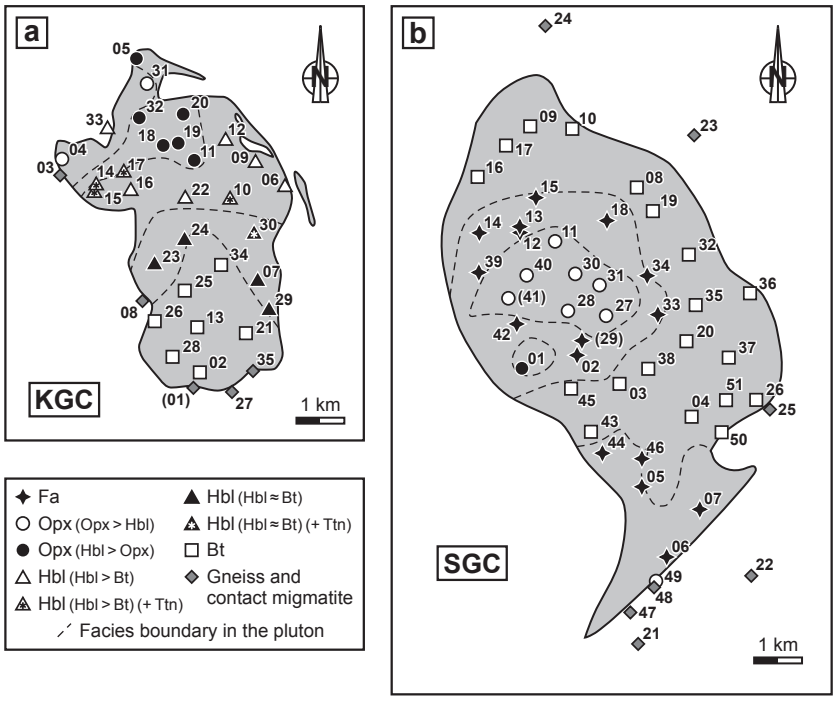

Fig. 4. Distribution map of the lithofacies, with location of the AMS sampling sites in (a) the KGC and (b) the SGC. Numbers (01, …) correspond to specimen numbers (KL01, …; SJ01, …), digits in brackets indicating samples not used for the AMS analysis. The boundaries between rock facies are from Petersen (1980) in (a) and from Maijer et al. (1994) in (b), modified according to our microscope observations.

in the NW, a hornblende granite (Hbl-facies) crops out in the centre and a biotite leucogranite (Bt-facies) occupies the southern part of the complex. This zoning is gradational: the transition from the Opx-facies to the Hbl-facies then to the Bt-facies is marked by a southward progressive increase of the hornblende *vs.* orthopyroxene ratio then of the biotite *vs.* hornblende ratio (Fig. 4a). All these rocks have a centimetric grain size. A fine-grained leucogranitic facies, containing biotite, orthopyroxene, garnet and sillimanite, forms a narrow strip along the southern contact of the KGC. This facies is intermingled with pegmatite pods and sheets, and often contains abundant and locally contiguous angular enclaves of mafic gneiss. Formerly considered as a late fractionation product of the KGC (Petersen, 1980; Jacamon and Larsen, 2009), this facies is here reinterpreted, due to its peculiar mineralogy and field aspect, as an equivalent of the contact migmatite.

Two coarse-grained, centimetric in grain size, contrasted rock types can be distinguished in the SGC (Fig. 4b): a quartz mangerite (orthopyroxene quartz monzonite) in the centre and southern portion of the complex, and a biotite leucogranite in the rest of the pluton. The quartz mangerite contains fayalite and is thus here referred to as Fa-facies, except in two areas of the central part of the SGC where this mineral is absent and which are petrographically similar to the Opx-facies of the KGC. The biotite leucogranite is rather similar to the Bt-facies of the KGC with, however, a common porphyritic texture. Crosscutting relationships and xenoliths in the SGC were taken by Maijer et al. (1994) as an evidence for the Fa- and Opx-facies to be younger than the Bt-facies and representing a separate intrusion. Age relationships will be confronted below with our results of the U-Pb dating and AMS investigation.

Decimetre- to m-large gneiss xenoliths are observed in the NW "bulge" and the NE part of the KGC where large roof pendants are present (Fig. 2; Petersen, 1977, 1980), as well as in the western central portion and near the eastern margin of the SGC. Fine-grained biotite- or hornblende-bearing granitic dyke-like bodies and lenses (grain size ~1 mm) varying in thickness from a few cm to 20–30 cm are ubiquitous in the SGC. The dyke-like bodies would be early intrusive features, as suggested by their variable orientation, as well as undulating to lobate contacts carrying aggregates of Fe-Mg minerals. Small dm-sized pegmatitic pods and dykes occur sporadically in both plutons.

Coarse-grained rock-facies of the KGC and SGC exhibit a penetrative and usually well-marked foliation mainly defined by a shape-preferred orientation of feldspars and mafic aggregates. The local occurrence of stretched quartz grains is consistent with a relatively strong imprint of a solid-state, ductile deformation (Vernon, 2000). In the two granitic complexes, the foliation pattern is rather homogeneous with dips dominantly steep and strikes following pluton margins (Figs. 2, 3). The weighted average of the mesoscopic foliation is similar for the two plutons, N155°E/89°WSW for the KGC and N145°E/83°NE for the SGC. A linear fabric defined by the shape-preferred orientation of mafic aggregates and orientated at N75°E/35°E is locally displayed in the NW bulge of the KGC. The gneiss xenoliths are always concordant with the mesoscopic foliation. The fine-grained, granitic dyke-like bodies and lenses in the SGC are either parallel or oblique to the foliation and, despite their variable orientation, a certain concentration around ENE-WSW strikes and moderate NNW dips can be defined.

5. Sampling procedure

A total of 86 samples was collected from the two granitic complexes, 35 samples for the KGC and 51 samples for the SGC (Fig. 4). The samples are homogeneously distributed across the outcropping areas (~1 sampling site/km^2) and include some rocks collected in the country rocks as well as from meter-thick outliers interbedded in the gneisses, namely KL33 close the NW contact of the KGC and SJ49 near the southern margin of the SGC. Most samples consist of orientated blocks from which 25-mm-diameter cores (usually two cores per sample) were drilled and then reorientated in the laboratory. Samples SJ01 to SJ16 were directly drilled and orientated in the field with a portable drill, usually two 25-mm-diameter cores per sampling site, and are paired with non-oriented hand samples collected at the same sites. Samples KL01, SJ29 and SJ41 are non-orientated blocks.

The AMS measurements were conducted on all orientated cores. A selection of hand samples was used for the other investigations (U-Th-Pb zircon dating, thermomagnetic and hysteresis measurements, image analysis). The analytical methods are detailed in Appendix 1.

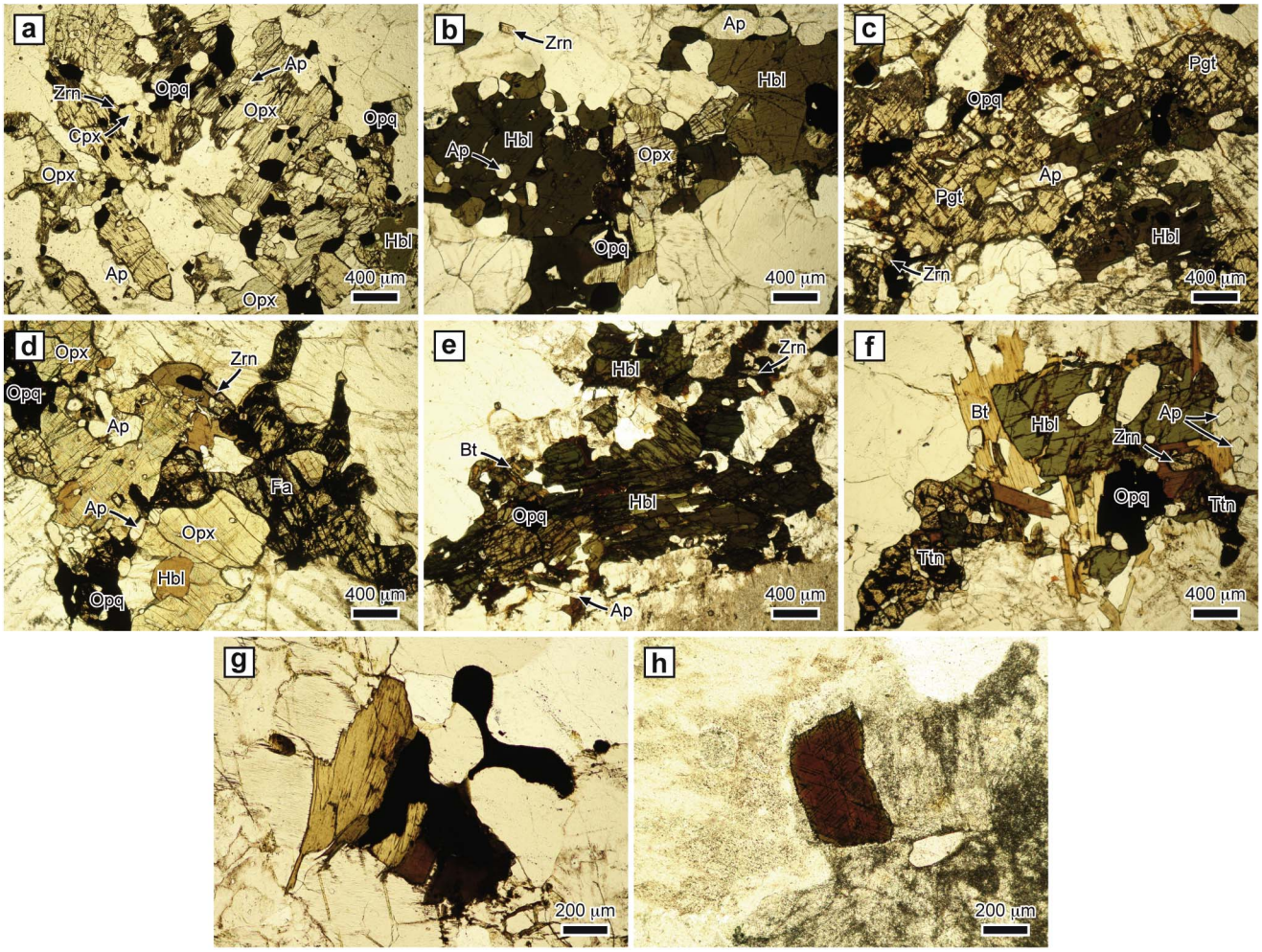

Fig. 5. Photomicrographs (transmitted light, uncrossed nicols) illustrating the mafic mineralogy. (a) Aggregate of primary orthopyroxene grains and subordinate opaque phase, hornblende, clinopyroxene, apatite and zircon (KL04; Opx-facies with Opx content > Hbl content, KGC); (b) large oikocrysts of hornblende aggregated with grains of primary orthopyroxene, apatite and opaque phase (KL05; Opx-facies with Hbl > Opx, KGC); (c) oikocrysts of inverted pigeonite and hornblende containing inclusions of opaque phase, apatite and zircon (note alteration of orthopyroxene) (SJ40; Opx-facies with Opx > Hbl, SGC); (d) aggregate of orthopyroxene and fayalite, and minor opaque phase, hornblende, apatite and zircon (SJ02; Fa-facies, SGC); (e) hornblende grains aggregated with subordinate biotite, opaque phase, apatite and zircon (KL09; Hbl-facies with Hbl > Bt, KGC); (f) aggregate of hornblende, biotite, titanite, and minor opaque phase, apatite and zircon (KL10; Ttn-subfacies with Hbl > Bt, KGC); (g) small aggregate of biotite crystals and opaque grains (KL26; Bt-facies, KGC); (h) sagenitic biotite isolated in a felsic matrix (SJ09; Bt-facies, SGC). Symbols: Ap, apatite; Bt, biotite; Cpx, clinopyroxene; Fa, fayalite; Hbl, hornblende; Opq, opaque mineral; Opx, (primary) orthopyroxene; Pgt, (inverted) pigeonite; Ttn, titanite; Zrn, zircon.

6. Petrography and microstructures

6.1. Rock-facies and texture

Alkali feldspar, plagioclase and quartz are the main minerals, and magnetite, ilmenite, sulfides (mostly pyrite), apatite and zircon are ubiquitous accessory minerals. Primary orthopyroxene associated with inverted pigeonite in the SGC, clinopyroxene, fayalite, hornblende and biotite are present in variable amounts, according to lithology. In the Opx-facies, the Fe-Mg silicates are orthopyroxene, hornblende and subordinate clinopyroxene, the hornblende *vs.* orthopyroxene ratio increasing progressively southwards in the KGC (orthopyroxene content > hornblende content in the north and hornblende > orthopyroxene in the south; Figs. 4a, 5a, b), whereas orthopyroxene is usually dominating over hornblende in the SGC (Figs. 4b, 5c). In the Fa-facies (SGC), the Fe-Mg silicates are fayalite, orthopyroxene, hornblende, and minor clinopyroxene and biotite (Fig. 5d). The Hbl-facies (KGC) contains hornblende and biotite, and no pyroxene. It is characterized by a southward progressive increase of the biotite *vs.* hornblende ratio (hornblende content > biotite content in the north and hornblende ≈ biotite in the south; Figs. 4a, 5e, f). In the Bt-facies, biotite (sagenitic in the SGC) is the only Fe-Mg silicate (Fig. 5 g, h). In the KGC, the proportions of biotite in this facies decrease sharply towards the south, down to very low values (< 1%) near the pluton margin. Some accessory minerals are found exclusively in the KGC, namely fluorite observed locally in the Hbl- and Bt-facies, and titanite present in the Hbl-facies, in two distinct areas of the pluton (Figs. 4a, 5f), which led us to define a Ttn-subfacies. Allanite is a common accessory mineral in the KGC and is rare in the SGC.

The average grain size is in the range 2–8 mm. Prismatic feldspar phenocrysts up to 5 cm-long are found locally in the Opx- and Fa-facies, and are common in the Bt-facies of the SGC. Fe-Mg silicates and other accessory minerals tend to form more-or-less elongated clusters (Fig. 5a–g), with locally oikocrysts of orthopyroxene and hornblende containing inclusions of opaques, apatite and zircon (Fig. 5b, c).

6.2. Opaque mineralogy

Magnetite is a titanomagnetite that commonly contains oxidation-exsolution lamellae of ilmenite parallel to the {111} planes of the host (Duchesne, 1972; Dunlop and Özdemir, 2009), forming sandwich-like (Fig. 6a) or trellis-like (Fig. 6b) microstructures. In the Ttn-subfacies,

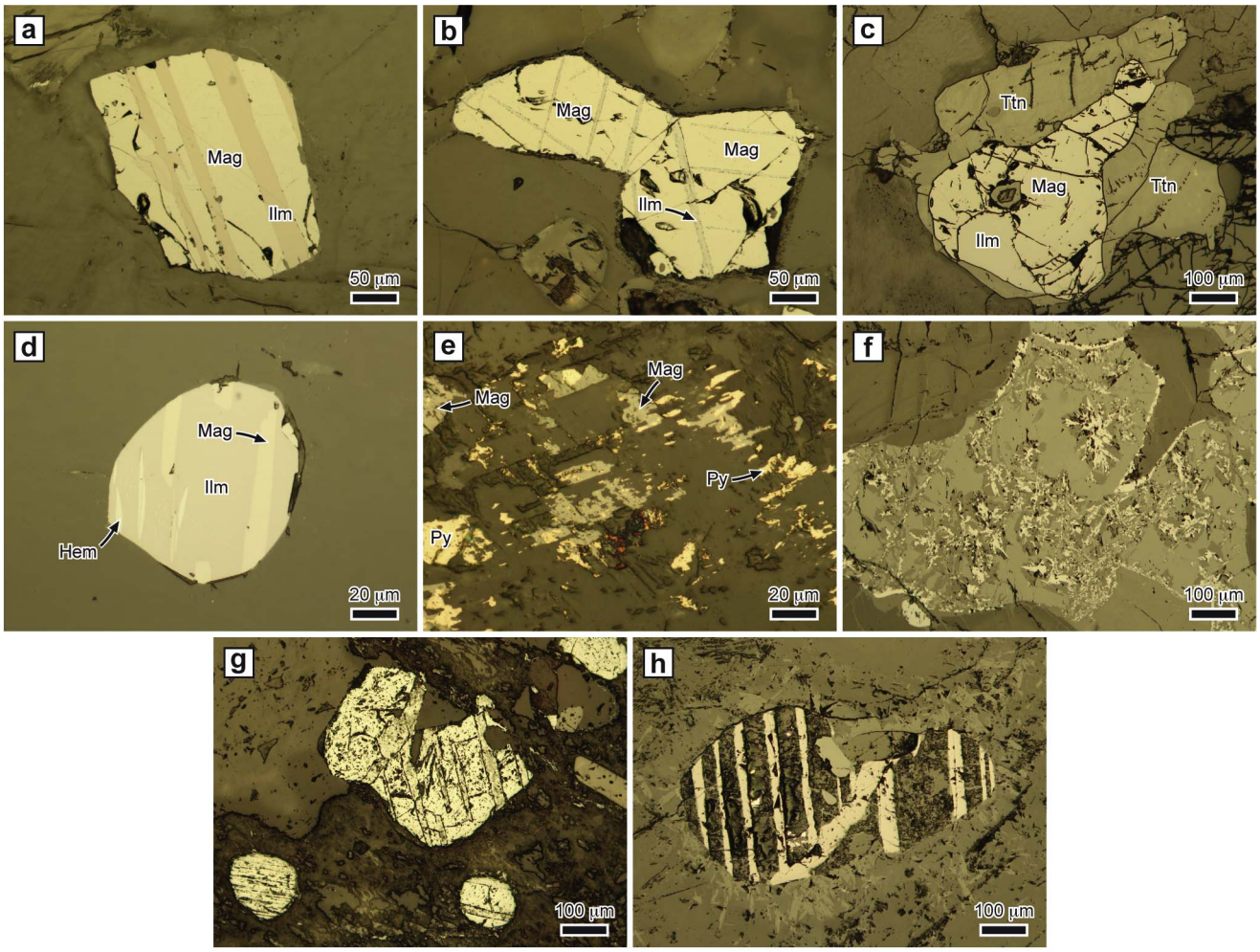

Fig. 6. Opaque mineralogy (photomicrographs taken in reflected light, uncrossed nicols). (a) Grain of titanomagnetite with relatively thick oxidation-exsolution lamellae of ilmenite (sandwich-like microstructure) (KL04; Opx-facies, KGC); (b) two adjacent grains of titanomagnetite showing a network of thin oxidation-exsolution lamellae of ilmenite orientated according two directions (trellis-like microstructure; note the microcrystals of aluminous spinel in the ilmenite lamellae, at the contact with the magnetite host) (SJ49; Opx-facies, SGC); (c) composite oxide area made of homogeneous (titano)magnetite and ilmenite, surrounded by a rim of titanite (KL15; Ttn-subfacies, KGC); (d) grain of hemo-ilmenite with reduction-exsolution lamellae of magnetite parallel to the exsolution lamellae of ilmenite (KL14; Ttn-subfacies, KGC); (e) patchy areas of secondary magnetite and pyrite in an altered orthopyroxene (KL05; Opx-facies, KGC); (f) thin rim and small aggregates of secondary magnetite left after alteration of fayalite (SJ39; Fa-facies, SGC); (g) strongly oxidized titanomagnetite grains (the magnetite component is largely martitized and the ilmenite lamellae are leucoxenized) (KL06; Hbl-facies, KGC); (h) ghost titanomagnetite (the magnetite host is completely transformed into an undetermined dark mineral, the ilmenite lamellae being unaltered) (SJ06; Fa-facies, SGC). Symbols: Hem, hematite; Ilm, ilmenite; Mag, magnetite; Py, pyrite; Ttn, titanite.

many (titano)magnetite grains are surrounded by titanite. These grains are homogeneous (no ilmenite lamellae; Fig. 6c), suggesting diffusion of titanium during crystallization of the titanite rim. Ilmenite is also homogeneous, except in some Ttn-subfacies samples in which thin exsolution lamellae of hematite are present along the (0001) basal plane of the ilmenite. Some of these hemo-ilmenite grains contain reduction-exsolution lamellae of magnetite parallel to the hematite exsolutions (Fig. 6d; Robinson et al., 2013). Pyrite grains locally contain tiny chalcopyrite areas. Titanomagnetite, (hemo-)ilmenite and locally pyrite are also found as platy to acicular exsolutions in some large grains of plagioclase and alkali feldspar.

6.3. Secondary mineralogy

Minerals have suffered an alteration of variable degree, the SGC being, in average, more altered than the KGC. Alteration of silicates led to the formation of sericite, epidote, calcite, saussurite, chlorite, serpentine, uralitic and cummingtonitic amphibole and talc, accompanied by secondary opaque phases (magnetite, pyrite ± chalcopyrite, ilmenite) as segregations along cleavage and microcracks, as well as patchy areas (Fig. 6e, f). Alteration affects also the primary opaque phases: the magnetite areas located between ilmenite lamellae in titanomagnetite may be either oxidized (martitized) into hematite (Fig. 6g) or leached into secondary minerals, mostly chlorite in the SCG, forming “ghost titanomagnetites” (Fig. 6h); ilmenite may be transformed into rutile (leucoxenization; Fig. 6g); and pyrite grains are commonly partly to completely replaced by an iron hydroxyde and/or magnetite.

In addition, green biotite and stilpnomelane are present in the SGC, mostly in the Bt-facies. Both minerals are typical of the M4b Caledonian retrograde metamorphic phase and their occurrence results from the proximity of the Caledonian front (Verschure et al., 1980; Sauter et al., 1983), that probably also explains the higher alteration degree of the SGC compared to the KGC.

6.4. Microstructures

Quartz shows various degrees of ductile deformation and recovery in thin section, which enables to distinguish between three types of microstructures: type 1, characterized by unstrained to slightly strained (undulose extinction) quartz grains that can be considered as magmatic (Paterson et al., 1998); type 2, characterized by incipient quartz polygonization (quartz grains with subgrain microstructure coexisting with

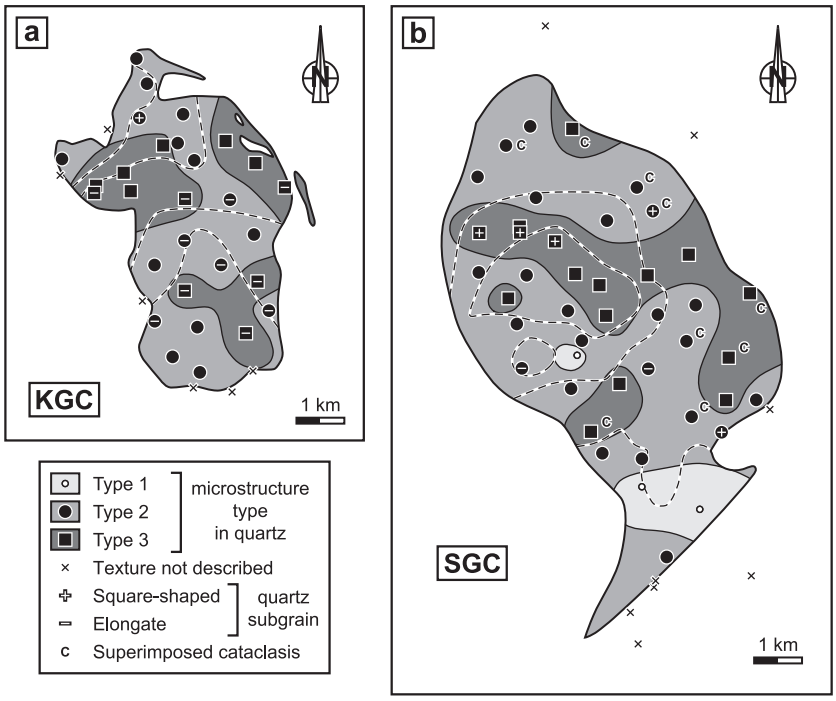

Fig. 7. Distribution map of the microstructures observed in (a) the KGC and (b) the SGC. Occurrence areas of the type 1, 2 and 3 quartz microstructures have been contoured inside the limits of the two plutons. Dashed lines: facies boundaries (see Fig. 4).

unstrained to slightly strained quartz); and type 3, with widespread recovery (all quartz grains divided into subgrains). Type 1 grains are scarce and found only in the Fa-facies (SGC), in small areas surrounded by type 2 microstructures (Fig. 7b). Type 2 and type 3 microstructures are present in both plutons, type 3 tending to concentrate in well-defined areas (Fig. 7). A roughly NW-SE-trending corridor of type 3 microstructures, running from the north to the centre of the SGC, is particularly worth noting (Fig. 7b).

The irregular, lobate boundaries of the quartz grains (typical of high-*T* grain boundary migration recrystallisation; Stipp et al., 2002), as well as the abundance of myrmekites developed a the expense of alkali feldspar (Passchier and Trouw, 2005) suggest that subsolidus deformation occurred at high temperature (> 500–600 °C). In the SGC, the dominant square or rectangular shape of quartz subgrains, giving rise to chessboard patterns (Figs. 7b, 8a), agrees with high-*T* conditions (Mainprice et al., 1986; Stipp et al., 2002). In the KGC, elongate subgrains in quartz are frequent (Figs. 7a, 8b), suggesting that deformation and recovery have lasted down to lower temperatures.

Additional evidence of ductile deformation, associated with type 2 and type 3 quartz microstuctures are undulose extinction in feldspar, weak curvature of polysynthetic twins and mechanical twinning (Fig. 8c) in plagioclase, and slight bending or kinking of cleavage in biotite (Fig. 8d) and primary orthopyroxene. Plagioclase-plagioclase boundaries and boundaries between grains of alkali feldspar are roughly rectilinear, often showing triple junctions with interfacial angles of ~120° (Fig. 8e), pointing to annealing during static recrystallization.

A low-*T*, brittle deformation is present in the Bt-facies of the SGC: almost a half of the samples from this facies (Fig. 7b) show a variable degree of cataclasis ranging from grain refinement along microfractures in feldspars and quartz (Fig. 8e), through cataclasis within mm-to-cm-wide zones (Fig. 8f), to complete crushing (sample SJ43). Cataclasis is accompanied by crystallization of secondary minerals (calcite, epidote, sericite, saussurite, chlorite and/or stilpnomelane). The occurrence of stilpnomelane indicates that cataclasis was coeval with the M4b Caledonian metamorphism.

7. Geochronology

CA-ID-TIMS U-Th-Pb analyses were performed on several single zircons in samples KL04 (Opx-facies; 7 grains), KL14 (Ttn-subfacies; 7 grains), SJ02 (Fa-facies; 7 grains) and SJ16 (Bt-facies; 8 grains). The results are reported in Appendix 2.

All the analyses are concordant to slightly discordant (Fig. 9). The centroid of most analyses plots marginally below the concordia curve, even after correction for ^{230}Th disequilibrium in the decay chain. The ^{207}Pb/^{206}Pb dates range from 938.7 ± 1.4 Ma to 946.4 ± 1.0 Ma for sample KL04 (age dispersion, Δ = 7.7 Ma), 937.7 ± 2.3 Ma to 946.5 ± 2.1 Ma for KL14 (Δ = 8.8 Ma), 935.0 ± 3.3 Ma to 948.4 ± 3.5 Ma for SJ02 (Δ = 13.4 Ma) and 936.3 ± 1.5 Ma to 1010.3 ± 1.4 Ma for SJ16 (Δ = 74.0 Ma) (all uncertainties at 2σ level). The ^{206}Pb/^{238}U dates are slightly younger and reduce the dispersion to, respectively, 6.35 Ma, 6.01 Ma, 7.10 Ma and 72.7 Ma. The dispersion of dates for each sample is larger than analytical uncertainty and therefore geologically meaningfull. It may reflect (*e.g.* Schaltegger et al., 2009; Barboni et al., 2013): occurrence of xenocrystic (*i.e.* inherited) zircon grains or zircon cores, older zircons that crystallized in the same magmatic system prior to emplacement (antecrystic grains), post-emplacement growth of autocrystic magmatic zircon and post-crystallization loss of radiogenic Pb. The dispersion of dates is relatively homogeneous, except in sample SJ16 where
six, slightly discordant grains ranging from 971.5 ± 1.7 Ma to 1010.3 ± 1.4 Ma are much older than two grains in the 935–940 Ma interval. These older grains plot within the time span known for the regional M1 metamorphic phase (1.035–0.97 Ga) and therefore are interpreted as xenocrystic zircons. Such a metamorphic origin is confirmed by the low Th/U ratios for these grains (0.10–0.11) compared to the other grains (0.20–1.36, for SJ16 and the three other analyzed samples). Low Th/U ratio is very common for zircon crystallization or recrystallization in a metamorphic environment (Hoskin and Schaltegger, 2003). With the exception of the xenocrystic zircons, analyses are interpreted to be related to crystallization of magmatic zircons.

Given the small size, hence heat content, of the KGC and SGC, it is unrealistic to attribute the large dispersion of the magmatic dates (up to 13.4 Ma) in samples KL04, KL14 and SJ02 to post-emplacement zircon

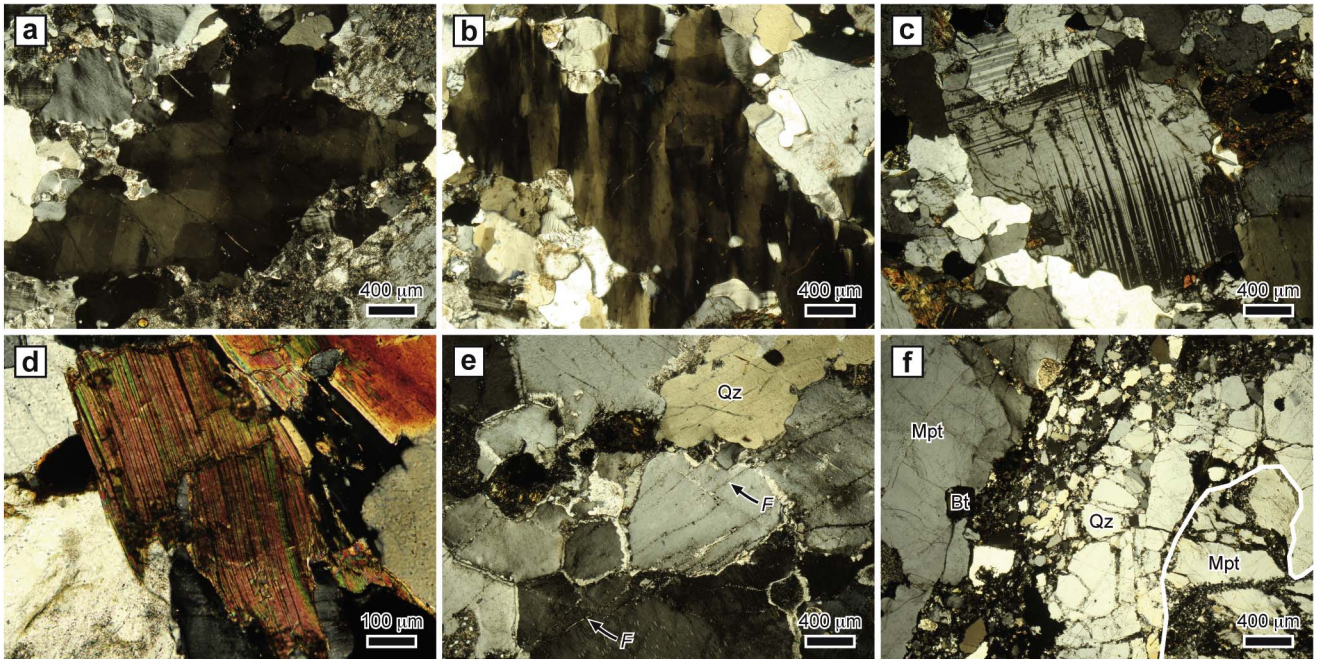

Fig. 8. Deformation, recovery and recrystallization microstructures in silicates (photomicrographs taken in transmitted light, crossed nicols). (a) Quartz grain divided into square-shaped subgrains (SJ50; Bt-facies, SGC); (b) quartz grain divided into elongated subgrains (KL15; Ttn-subfacies, KGC); (c) plagioclase grain with mechanical twins (SJ40; Opx-facies, SGC); (d) kinking of a biotite grain (KL17; Ttn-subfacies, KGC); (e) recrystallized polygonal microperthite grains, with boundaries tending to make triple junctions at ~120° (note border reactions between feldspar grains, as well as cataclasis along microcracks) (SJ19; Bt-facies, SGC); (f) cataclastic zone cutting across grains of quartz and microperthite (the white line marks the original boundary of a crushed microperthite grain; feldspar areas to the left are intact) (SJ20; Bt-facies, SGC). Symbols: Bt, biotite; F, cataclastic microcrack; Mpt, microperthite; Qz, quartz.

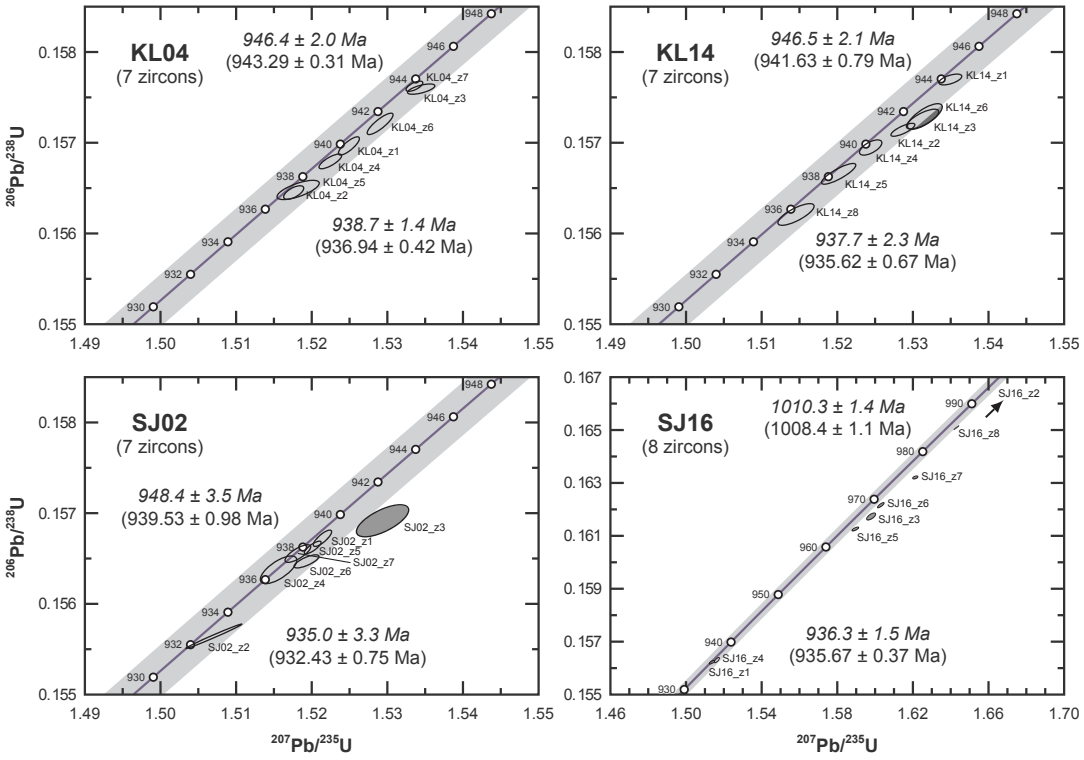

Fig. 9. Concordia diagrams with results of U-Th-Pb dating of zircons from the Opx-facies (KL04) and Ttn-subfacies (KL14) of the KGC, and from the Fa-facies (SJ02) and Bt-facies (SJ16) of the SGC. Note that for SJ16, the scale of the diagram axes is different, making the concordia error envelope thinner and the error ellipses smaller. The youngest and oldest zircon ages are indicated for each sample (ages in italic are $^{207}Pb/^{206}Pb$ dates and ages in brackets are $^{206}Pb/^{238}U$ dates).

crystallization. Such a dispersion is best attributed to the presence of antecrystic zircons. This interpretation carries two implications: (1) the youngest dates can be taken as a good approximation of the emplacement ages of the magmatic pulses (*e.g.* Schaltegger et al., 2009), and (2) the KGC (samples KL04 and KL14) and the quartz mangerite unit (Fa- and Opx-facies) of the SGC (sample SJ02) derived

Table 1
Thermomagnetic and hysteresis parameters.

Sample	K_m	T_V	T_M	T_C	T_N	Usp(%)	Ilm(%)	H_c	M_{rs}	M_s	Ferro(%)	
											Th	Hy
KL05	17.9	−157	–	570	–	1.4	–	0.7	21.7	909.8	98	100
KL06	0.26	−155 [w]	−18	575	676	0.5	0.5	120.7	7.7	20.8	94	90
KL13	2.9	−155	−7 [w]	573	673	0.9	0.8	0.7	4.8	350.1	100	100
KL14	84.0	−154	−10[c]	572	–	1.0	–	0.7	86.1	3596	100	100
SJ05	13.5	−154 [w]	–	571	–	1.2	–	0.7	4.7	224.8	100	98
SJ06	0.40	–	–	568	–	1.7	–	6.5	0.6	7.9	84	31
SJ11	19.5	−163	–	572	–	1.0	–	0.7	33.0	812.0	100	99
SJ32	8.5	−161	–	573	–	0.9	–	0.8	17.5	490.0	100	100
SJ37	0.23	–	–	563	672	2.6	0.9	0.7	0.03	1.8	33	31
SJ39	35.1	–	–	570	–	1.4	–	0.7	11.6	1424	100	100

K_m: magnitude of the bulk magnetic susceptibility (in 10^{-3}SI) (see Appendix 4); T_V and T_M: temperature of the Verwey and Morin transitions (in °C) estimated from cooling and warming induced magnetization *vs.* temperature curves (temperature corresponding to the highest value of the curve slope in the transition interval); T_C and T_N: Curie and Néel temperatures (in °C) estimated from warming magnetic susceptibility *vs.* temperature curve using the method of Petrovský and Kapička (2006); *Usp*(%): mole fraction of ulvospinel (in %) in titanomagnetite calculated from T_C after Clark (1997); Ilm(%): mole fraction of ilmenite (in%) in titanohaematite calculated from T_N after Clark (1997); H_c: coercivity (in mT); M_s: saturation magnetization (in mA m^2/kg); M_{rs}: saturation remanence (in mA m^2/kg); *Ferro* (%): ferromagnetic contribution (in %) to the low-field magnetic susceptibility (*Th*: estimated from susceptibility *vs.* temperature warming curve through the fitting method of Hrouda, 1994; *Hy*: estimated from hysteresis loop by subtracting susceptibility measured at high magnetic field from the low-field susceptibility).
Note: all hysteresis parameters (H_c, M_s, M_{rs}) correspond to adjusted hysteresis loops after high-field slope correction.
[W]Verwey or Morin transition observed only in the warming curve.
[C]id. only in the cooling curve.

from silicate melts with a protracted history (~8 Ma in average) from their genesis at depth to their emplacement and crystallization. The youngest detected zircon in each sample has a negligible degree of discordance (Fig. 9), hence the corresponding $^{206}Pb/^{238}U$ date is much more accurate than the $^{207}Pb/^{206}Pb$ date and considered as the best estimate for magma emplacement: 936.94 ± 0.42 Ma for KL04, 935.62 ± 0.67 Ma for KL14, 932.43 ± 0.75 Ma for SJ02 and 935.67 ± 0.37 Ma for SJ16.

All these emplacement ages overlap the U-Pb dates previously obtained for the AMC (932–916 Ma) and HBG suites (957–926 Ma in the RVA sector) (Schärer et al., 1996; Vander Auwera et al., 2011, 2014). They improve previously published Rb-Sr dates: 911 ± 3 Ma for the KGC (Rb-Sr whole-rock age; recalculated from Petersen and Pedersen, 1978), ~930–900 Ma for the quartz mangerite unit of the SGC (estimation of Maijer et al., 1994 from Rb-Sr whole-rock and mineral isochrons) and 985 Ma ± 165 Ma for the Bt-facies of the SGC (Rb-Sr whole-rock age; Maijer et al., 1994). A preliminary U-Pb zircon date of 937 ± 3 Ma found by Sauer (2011) for the Fa-facies (SGC) is close to the U-Pb age of sample SJ02 (932.43 ± 0.75 Ma). A U-Pb zircon date of 1027 ± 9 Ma published by Coint et al. (2015) for the Bt-facies of the SGC was interpreted by these authors as an emplacement age and, consequently, taken as an evidence to connect this part of the granitic complex with the 1.06–1.02 Ga Sirdal magmatic belt. We consider that this age relates to the occurrence of xenocrystic zircons, as shown in sample SJ16.

Actually, the SGC components represent penecontemporaneous magmatic pulses, the Bt-facies being slightly older by ~3.2 Ma than the rest of the pluton, as demonstrated by the non-overlapping emplacement ages of SJ16 (935.67 ± 0.37 Ma) and SJ02 (932.43 ± 0.75 Ma). Hence, the field observations of Maijer et al. (1994) suggesting that the Bt-facies of the SGC is older than the Fa- and Opx-facies are corroborated by the U-Pb geochronological data (the Rb-Sr dates, despite their large uncertainties, were also viewed by these authors as an argument for two separate intrusions, with, however, a much larger time gap than the one found here). As a consequence, the SGC experienced a moderately long construction time with a marked repose period between emplacement of the Bt-facies and injection of the Fa- and Opx-facies across the first magmatic pulse. The slightly overlapping emplacement ages of the Opx-facies (936.94 ± 0.42 Ma) and Ttn-subfacies (935.62 ± 0.67 Ma) in the KGC confirm its building by more-or-less coeval magma batches (Petersen and Pedersen, 1978; Petersen, 1980) within a shorter time interval than the SGC (≲1 Ma), justifying the transitional character from one rock facies to another in this pluton. We note that the magmatic pulses that formed the KGC are almost coeval with the oldest portion, *i.e.* the Bt-facies, of the SGC.

8. Rock magnetic study

Thermomagnetic (MT) curves and hysteresis loops have been measured on ten samples from the KGC and SGC, representative of the range of measured susceptibility (KL05, 06, 13, 14; SJ05, 06, 11, 32, 37, 39). All the magnetic curves are reported in Appendix 3 and the corresponding parameters are given in Table 1. A selection of results is displayed in Fig. 10. The AMS data, *i.e.* the magnitudes and orientations of the three principal axes ($K_1 \geq K_2 \geq K_3$) of the AMS ellipsoid, are reported in Appendix 4.

8.1. Thermomagnetic and hysteresis measurements

A Curie point at 563–575 °C in the *MT curves*, associated in many cases with a faint Hopkinson peak (Fig. 10a), indicates a Ti-poor titanomagnetite (2.6–0.5 mol% of ulvospinel; Table 1). This almost pure magnetite is responsible, in most MT curves, for a Verwey transition at temperatures of −163 °C to −154 °C (Table 1; Fig. 10b). The abundance of ilmenite lamellae in the titanomagnetite grains (Fig. 6a, b), expression of the segregation between magnetite-rich areas and ilmenite lamellae related to Ti diffusion during oxy-exsolution (Dunlop and Özdemir, 2009), accounts for this near-end-member composition. An additional Ti depletion in the titanomagnetite likely occurred during formation of titanite reaction rims in the Ttn-subfacies (Fig. 6c). A minor decay is also observed in the MT curves at ~675 °C (Table 1; Fig. 10a) for the very low susceptibility specimens (KL06, KL13, SJ37). This is the Néel temperature characteristic of a titanohematite close to pure hematite (< 1 mol% of ilmenite; Table 1) corresponding to the optically identified secondary hematite particularly abundant in KL06 (Fig. 6 g). Occurrence of hematite explains the well-defined Morin transition in the MT curves of KL06 at −18 °C (Table 1; Fig. 10b). The paramagnetic contribution to magnetic susceptibility as estimated from the MT data (Table 1) is 6% for KL06, 16% for SJ06 and 67% for SJ37. For all other samples, this paramagnetic contribution is negligible (ferromagnetic contribution estimated at 98–100%; Table 1).

The S-shaped and narrow *hysteresis loops* obtained for most analyzed

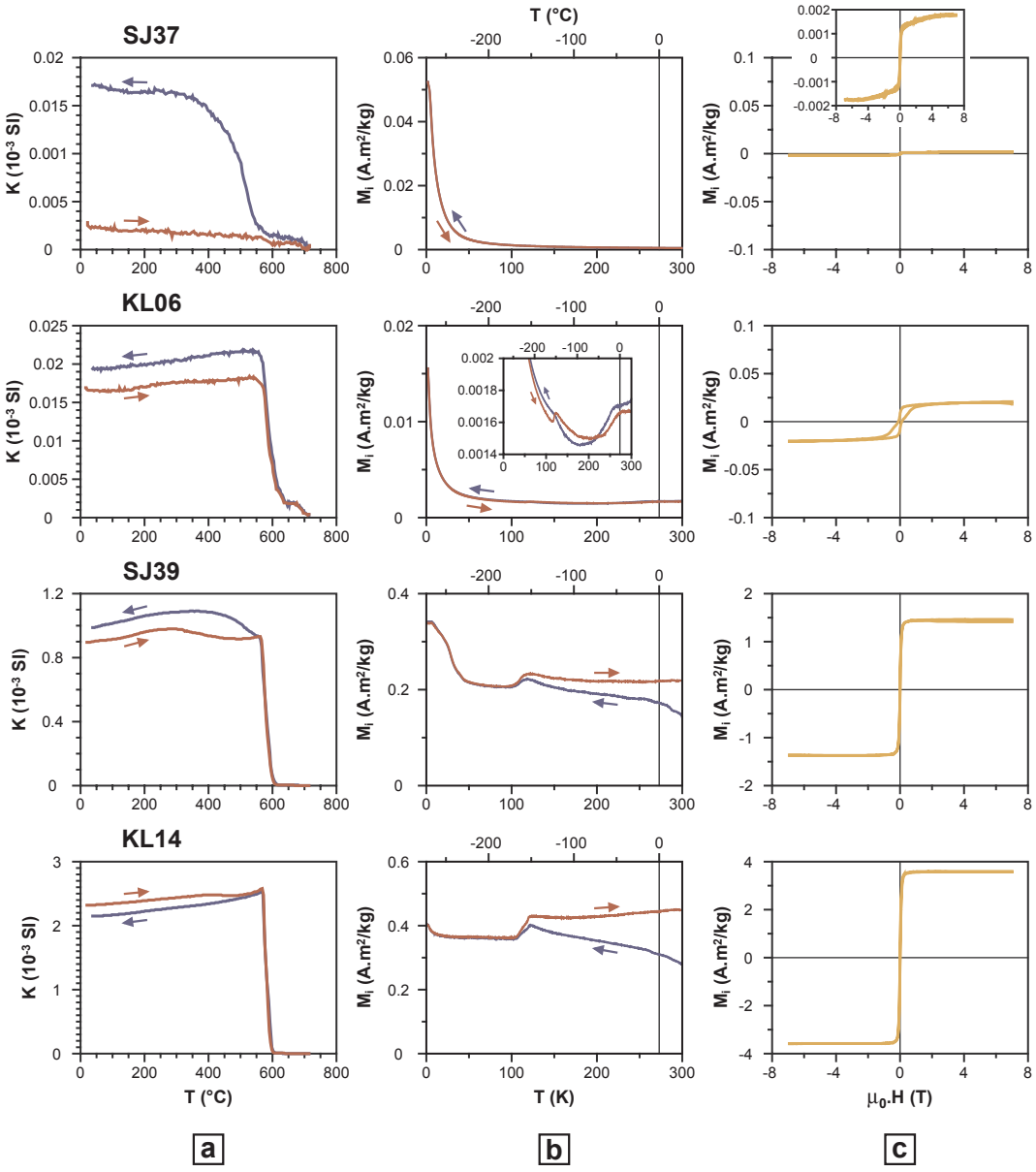

Fig. 10. Selected magnetic curves (KL06, KL14, SJ37, SJ39). (a) Magnetic susceptibility *vs.* temperature curve measured between room temperature and 715 °C; (b) induced magnetization *vs.* temperature curve measured between −271 °C and 27 °C; (c) hysteresis loop after high-field slope correction. The curves are ordered by increasing susceptibility values (K_m; see Appendix 4).

samples, and the values of their hysteresis parameters (Fig. 10c; Table 1) indicate a dominant ferromagnetic behaviour carried by multidomain "magnetite" (Dunlop and Özdemir, 2009), namely the already described Ti-poor titanomagnetite. The relatively abundant (secondary) hematite of specimen KL06 is responsible for a constriction in the hysteresis loop (Fig. 10c) together with a high coercivity (H_c) value (> 100 mT; Table 1). The ferromagnetic contribution to susceptibility as estimated from the hysteresis loops (Table 1) is 98–100%, except for KL06 (90%), SJ06 (31%) and SJ37 (31%), in agreement with the thermomagnetic results, with the notable exception of SJ06.

In short, the rock magnetic data, controlled by the petrographic observations, collectively indicate a magnetic mineralogy dominated by a multidomain, Ti-poor titanomagnetite in most samples. Exceptions concern very low susceptibility specimens, that have a non-negligible contribution of paramagnetic minerals and in which the ferromagnetic component may be due to secondary hematite in case of strong alteration (*e.g.* KL06).

8.2. AMS scalar parameters

Values of the *bulk magnetic susceptibility*, $K_m = (K_1 + K_2 + K_3)/3$, range from 0.10 to 84.0 × 10^{-3} SI in the KGC and from 0.04 to 64.2x10^{-3}SI in the SGC (Fig. 11a). Such large variations indicate variable mineral contributions to susceptibility, confirming the thermomagnetic and hysteresis data. Following the latter, the strongest paramagnetic contribution is observed in samples SJ06 (K_m = 0.40 × 10^{-3} SI) and SJ37 (K_m = 0.23 × 10^{-3} SI), suggesting that 0.5 × 10^{-3} SI can be considered as a limit above which susceptibility is dominantly ferromagnetic, as usually admitted (Rochette, 1987; Bouchez, 2000). Accordingly, 90% of the samples from the KGC and 68% from the SGC can be considered as having their susceptibility controlled by ferromagnetic minerals, namely magnetite. The two plutons are thus dominantly ferromagnetic, with the notable exception of the SGC Bt-facies in which only 37% of the samples have K_m > 0.5 × 10^{-3} SI. The granitic material of the contact migmatite to the south of the KGC has a low susceptibility (0.02–0.15 × 10^{-3} SI)

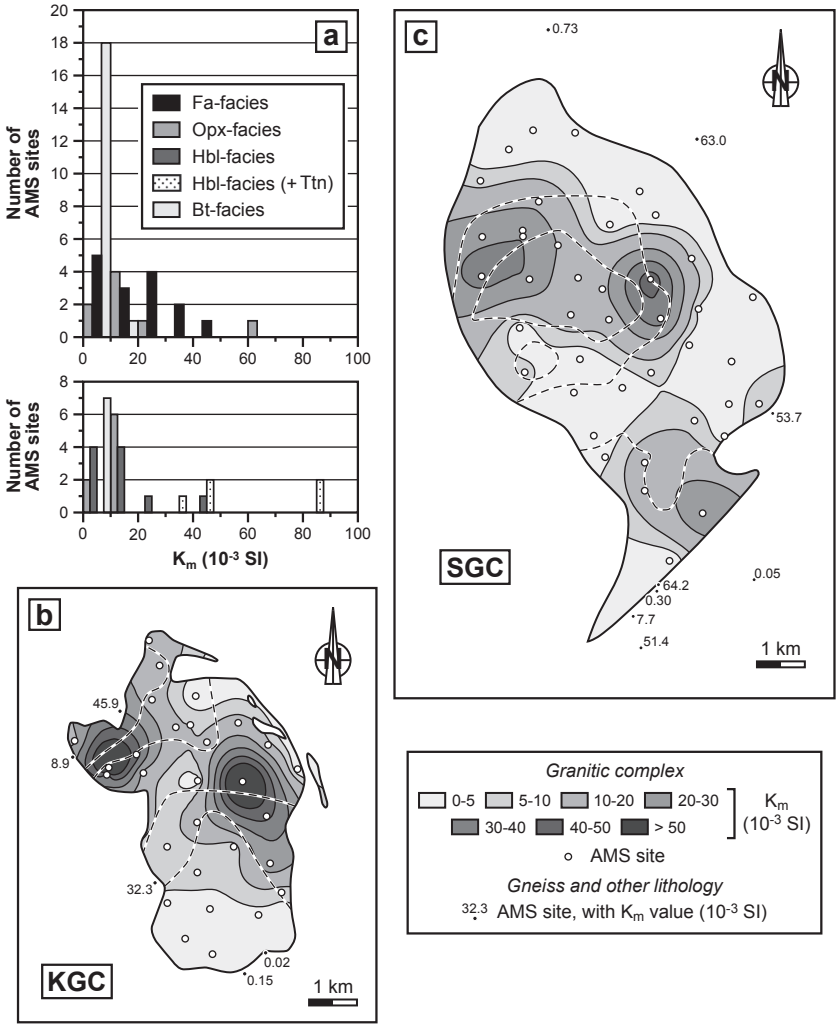

Fig. 11. Magnetic susceptibility (K_m). (a) Partial histogram of K_m within the KGC (bottom) and the SGC (top); (b) contoured map of K_m within the KGC (the other sampled lithologies are plotted with their own K_m value); (c) id. for the SGC. Dashed lines: facies boundaries (see Fig. 4).

controlled by paramagnetic minerals and the gneissic wall rocks of the two plutons have susceptibilities varying from paramagnetic to ferromagnetic (0.05–63.0 × 10^{-3} SI).

In details, (sub)facies of the KGC and SGC can be ordered by increasing K_m values as follows (Fig. 11a): Bt-facies (0.04–10.3 × 10^{-3} SI; 2.9 × 10^{-3} SI in average), Opx and Hbl-facies (0.26–28.5 × 10^{-3} SI; 13.0 × 10^{-3} SI in average; excluding the Ttn-subfacies, as well as outliers KL33 and SJ49 whose K_m value is, respectively, 45.9 × 10^{-3} SI and 64.2 × 10^{-3} SI), Fa-facies (0.40–47.4 × 10^{-3} SI; 19.1 × 10^{-3} SI in average) and Ttn-subfacies (38.4–84.0 × 10^{-3} SI; 58.8x10^{-3}SI in average). This correlation between susceptibility and petrographic type is illustrated on the contoured maps of K_m (Fig. 11b, c): zones of peak values are centred on the outcrop areas of the Ttn-subfacies in the KGC (K_m > 20 × 10^{-3} SI) and the Fa-facies in the SGC (> 10 × 10^{-3} SI), whereas in both complexes, zones with K_m < 5 × 10^{-3} SI coincide roughly with the Bt-facies. K_m as a proxy for rock composition is a usual feature in granitoids, both in paramagnetic and ferromagnetic lithologies (*e.g.* Gleizes et al., 1993; de Saint Blanquat and Tikoff, 1997; Román-Berdiel et al., 2004; Bolle et al., 2010).

Magnetic susceptibility is impacted by alteration through the formation of new mafic minerals and leaching of the primary ones (in particular, magnetite). The role played by secondary minerals is difficult to quantify. Leaching of primary magnetite may induce significant susceptibility decrease. For example, the strongly altered mafic minerals of sample KL06 (Hbl-facies) lead to very low susceptibility values (0.26 × 10^{-3} SI) compared to other samples coming from the same facies (2.2–45.9 × 10^{-3} SI, excluding Ttn-subfacies). Also, in the SGC, samples with numerous ghost magnetites have susceptibilities two to three times lower than those of less altered samples.

The P_j and T_j parameters of Jelínek (1981) are used here to describe, respectively, the *anisotropy degree and shape of the magnetic fabric*, with P_j ranging from zero (isotropic fabric, *i.e.* spherical ellipsoid) to higher values, and T_j varying from −1 (prolate uniaxial ellipsoid) to 1 (oblate uniaxial ellipsoid), through zero (neutral ellipsoid).

P_j and T_j vary, respectively, from 1.01 to 1.61 and −0.72 to 0.78 in the whole data set, indicating weakly to moderately anisotropic and strongly prolate to strongly oblate magnetic fabrics. Within the KGC and SGC, respectively, the P_j values are in the interval 1.02–1.61 (average of 1.21) and 1.01–1.25 (average of 1.12), and the T_j values vary from −0.63 to 0.68 (average of −0.13) and from −0.72 to 0.55 (average of -0.02). In average, the magnetic fabric is thus stronger in the KGC than in the SGC, and it is slightly prolate in the former and roughly neutral in the latter.

The P_j–K_m plot (Fig. 12a, b) suggests that the anisotropy degree is influenced by the susceptibility, as usually observed both in ferromagnetic and paramagnetic granitoids (Bouchez, 2000; Ferré et al., 2014; among others). This correlation has been attributed by Ferré et al. (2014) to variations of the magma viscosity with the iron content (magmas having a higher iron content, hence a lower viscosity would record a higher shear strain, hence a higher anisotropy degree). The positive correlation between P_j and K_m is confirmed by the rather good fit between zones of maximum values on the contoured maps of K_m (Fig. 11b, c) and P_j (Fig. 13a, b). However, this agreement between maps is not perfect, especially for the SGC, suggesting that the

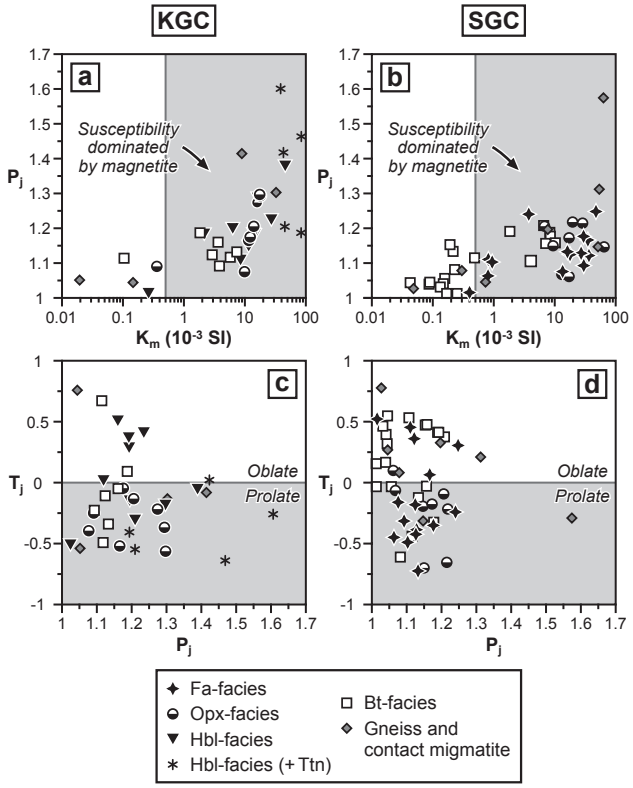

Fig. 12. Correlation diagrams of K_m, P_j and T_j. (a) Plot of P_j *vs.* K_m for data within and around the KGC; (b) id. for the SGC; (c) plot of T_j *vs.* P_j for data within and around the KGC; (d) id. for the SGC.

anisotropy also relates to the amount of strain undergone by the rocks. The competing effect on the anisotropy degree between magnetic susceptibility and deformation has been observed in other granitoids from southernmost Norway (Bolle et al., 2003, 2010).

The T_j–P_j plot illustrates the dominance of prolate fabrics in the KGC (Fig. 12c) and the roughly symmetrical distribution of ellipsoid shapes on both sides of the $T_j = 0$ threshold for the SGC (Fig. 12d). Except the tendency for the strongest magnetic fabrics to be neutral to prolate in shape, no obvious correlation between T_j and P_j is observed. The K_m (Fig. 11b, c) and T_j (Fig. 13c, d) contoured maps, when compared to each other, indicate that the shape of the magnetic fabric is not related to the magnetic susceptibility, further suggesting that the shape factor is perhaps more influenced by strain than the anisotropy degree. Interestingly, the contouring of T_j shows that moderately to strongly prolate magnetic fabrics ($T_j < -0.5$) in the KGC are observed only in the NW bulge of the pluton, where lineation locally dominates the petrofabric.

8.3. AMS directional data

Magnetic foliations (K_1K_2 planes) in the KGC, whose weighted average is N18°E/64°ESE, are NNE-SSW striking with moderate to steep dips to the east in the western part of the pluton (Fig. 14a). At the southern end and in the eastern part of the complex, foliation strikes are parallel to the pluton margins, with steep southern dips in the south and increasing SW dips towards pluton core in the east. Foliations, especially in the pluton western part, are more-or-less concordant with the magnetic and the gneissic foliations measured in the high-grade country rocks. We note also that foliation trajectories at the pluton contact define three neutral zones in the wall rocks (Fig. 14a).

The pattern of magnetic lineations (K_1 axes) in the KGC (weighted average, N160°E/48°SSE) is more homogeneous (Fig. 14b), being gently to steeply plunging, from 9° to 69°, to the south, except in the central western part and southern end of the pluton where eastern plunges are observed. These magnetic lineations are concordant with the magnetic and the mineral or stretching lineations measured to the west of the complex. The mean lineation is, within a few degrees (6°), the same as the zone axis of the foliations poles that form an ill-defined great circle (Fig. 14a).

The pattern of magnetic foliations in the SGC (weighted average, N161°E/35°ENE) is relatively heterogeneous, with variable dips and strikes (Fig. 15a). However, foliations tend to follow the intrusive contacts of the complex, as observed in map view.

As for the KGC, the magnetic lineations in the SGC (weighted average, N127°E/23°SE) define a rather homogeneous pattern (Fig. 15b), being gently to steeply plunging, from 5° to 65°, dominantly to the north-east, east or south and, locally, to the opposite direction (SW to north). The NW-SE-trending corridor of type 3 microstructures in the northern and central parts of the SGC (Fig. 7b) is parallel to the lineation pattern of the area. The mean lineation is very close (12°) to the zone axis of the ill-defined girdle displayed by the foliation poles (Fig. 15a). Magnetic lineations measured in the gneisses are mostly concordant with their neighbours in the SGC.

In both complexes, the lineation trajectories are roughly parallel to pluton elongation, and, at many places, cut across both the internal contacts and pluton margins. The foliation trajectories also cut across the facies boundaries. However, in the northern part of the SGC, the fabrics are discordant on both sides of the boundary between the Bt-facies and the central quartz mangerite zone (Fig.15).

9. Significance of the magnetic fabric: Image analysis contribution

Discrepancies between the magnetic foliation and the foliation measured in the field are observed at many AMS sites. The largest inconsistencies (> 60°) occur in the NW part of the KGC (compare Figs. 2 and 14a) and in the east of the SGC, in the Bt-facies (compare Figs. 3 and 15a). The magnetic lineation measurement complies with that of the only field lineation measured in the KGC (site KL15; compare Figs. 2 and 14b).

The common discrepancy between magnetic foliations and field measurements justifies the use of a 3D image analysis to investigate the relationship between the magnetic fabric and the shape fabric of the minerals. Nine oriented blocks from the KGC and SGC displaying variable discordances between the magnetic and the mesoscopic foliation (KL05, 16, 30; SJ17, 26, 27, 32, 33, 39) were therefore subjected to an image analysis. Raw data are given in Appendix 5 and compared with the AMS data in Fig. 16.

In the nine samples, discrepancies between the shape fabric of the analyzed minerals and the corresponding magnetic fabric are low to moderate (2° to 40°), the largest ones (> 20°) occurring in samples whose either the shape fabric or the magnetic fabric has a well-marked prolate ($T_j < -0.30$) or oblate ($T_j > 0.30$) character. An extreme example is provided by KL16 that has a weakly prolate magnetic fabric ($T_j = -0.16$) and a moderately prolate shape fabric ($T_j = -0.52$), with consequently subparallel long principal axes (deviation of 2°), and large departures (~40°) between the intermediate and the short axes. Not surprisingly, misorientation between magnetic fabric and shape fabric relies thus mostly on the symmetry of the AMS and shape ellipsoids.

The image analysis study thus supports the use of AMS as a proxy for the orientation of the petrofabric (Fig. 16), even where the magnetic and the mesoscopic-scale foliations are discordant, as observed in particular in the NW of the KGC (see KL05, KL16) and in the east of the SGC (see SJ26). The latter discrepancies probably reflect inaccurate measurements of the mesoscopic foliation, due either to the prolate character of the shape fabric, as best illustrated in the NW bulge of the KGC (*e.g.* $T_j = -0.52$ for the shape fabric of KL16) or to a foliation that

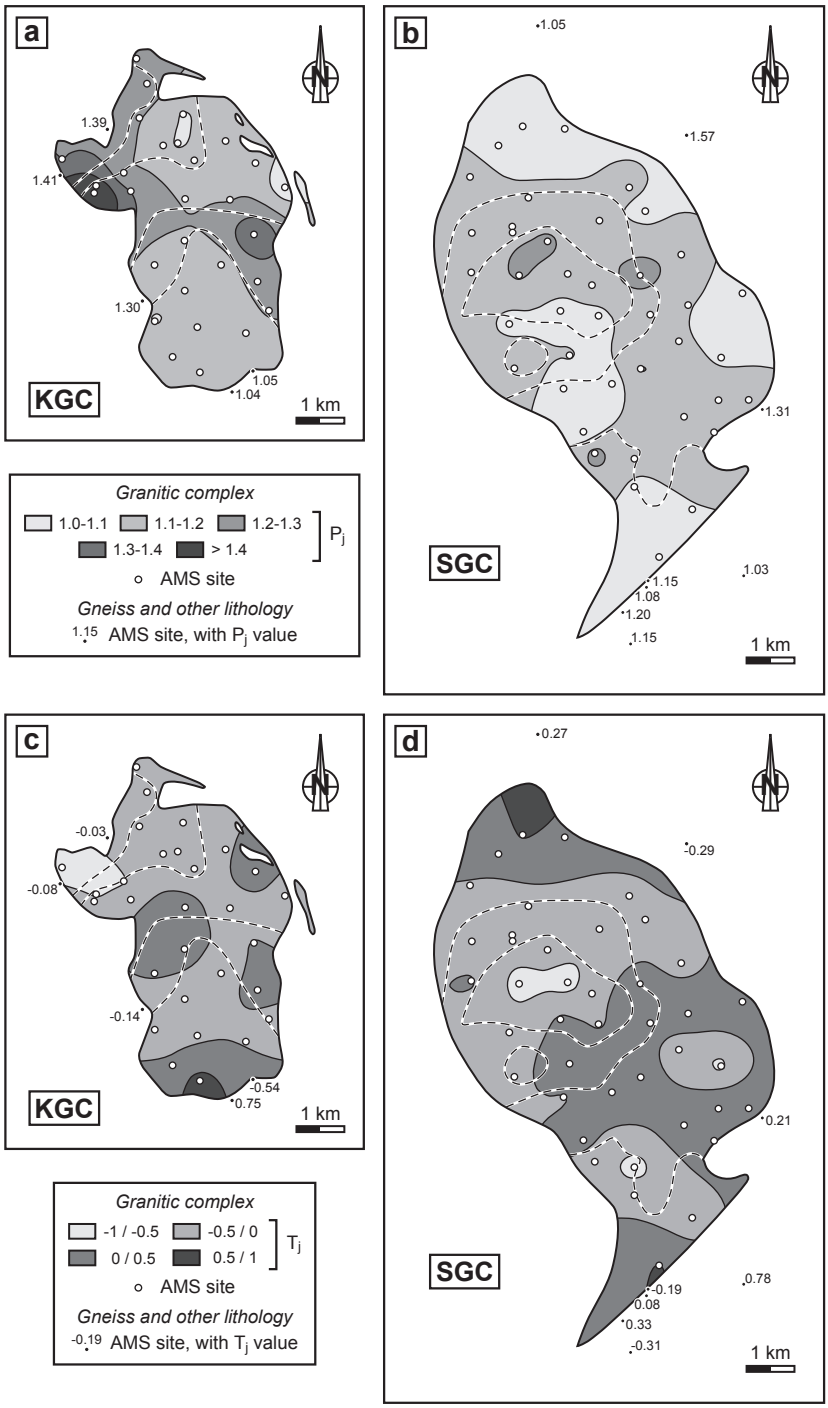

Fig. 13. Map view distribution of P_j and T_j in the plutons and surrounding gneisses. (a) P_j in the KGC; (b) id. for the SGC; (c) T_j in the KGC; (d) id. for the SGC. Dashed lines: facies boundaries (see Fig. 4).

is less well defined than usual, which could apply to the Bt-facies, in the east of the SGC.

For the SGC, results of the image analysis further show that the Caledonian overthrusting and associated metamorphism (M4b) responsible for quite severe alteration and local cataclasis in the pluton did not modify significantly the orientation of the magnetic fabric. In particular, leaching of primary magnetite, responsible for a significant susceptibility decrease in many SGC samples, was not so thorough as to have destroyed the primary magnetic fabric. The only proven case of discordance between magnetic and mesoscopic foliations due to an abnormal, secondary magnetic fabric is that of sample KL06 from the KGC (Figs. 2, 14a) where strong alteration has deeply modified the magnetic mineralogy.

10. Fabric interpretation

10.1. Evidence of emplacement in a tectonic strain field

Field structural observations, such as well-defined foliations and occurrence of stretched quartz grains, and microscope evidence of weak but widespread intracrystalline deformation and recovery at high to lower temperature indicate that the two complexes were tectonically deformed (Vernon, 2000), probably during and just after crystallization. Emplacement in a tectonic strain field is further supported by the continuity of the fabric, especially the lineation, across the internal contacts and the pluton margins (Paterson et al., 1998), by the foliation passing locally through the granitic dyke-like bodies and lenses in the SGC, and by the neutral zones in the gneisses at the contact of the KGC

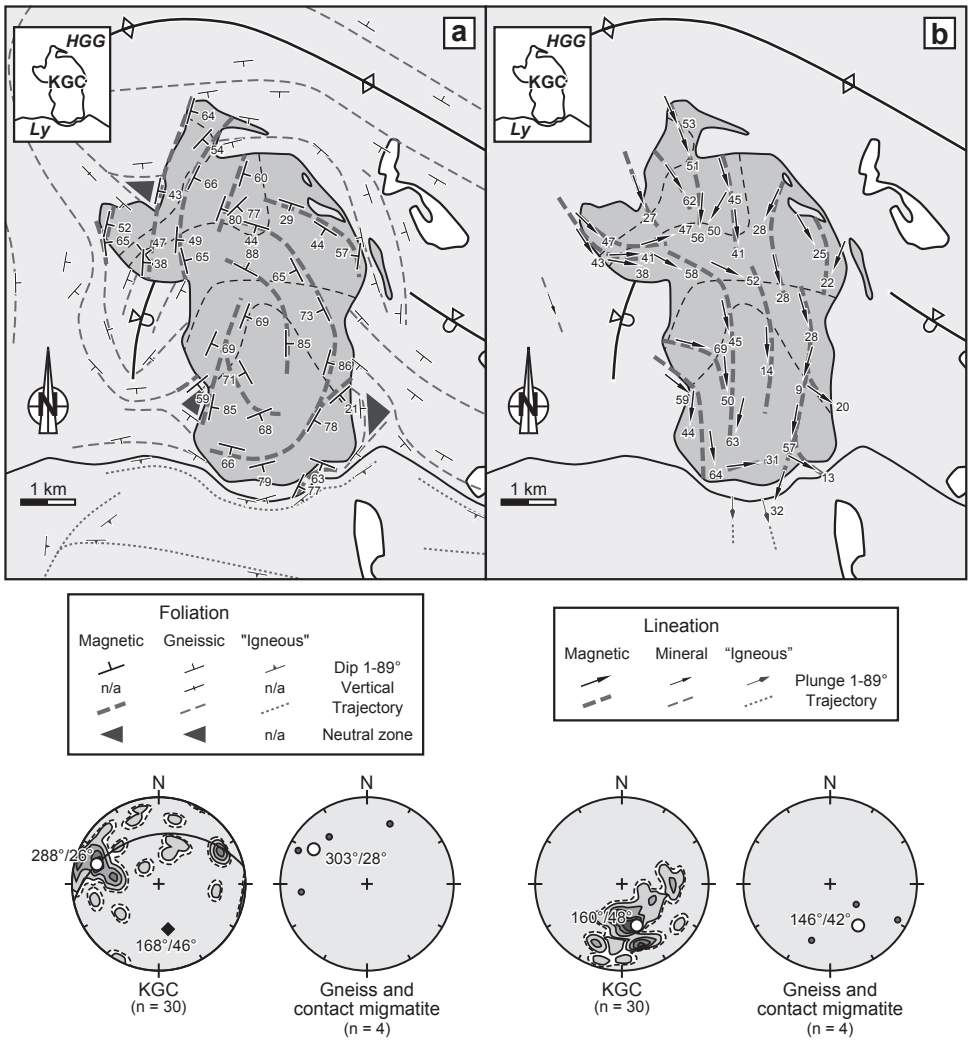

Fig. 14. Map of the magnetic (a) foliations and (b) lineations in the KGC, with lower hemisphere, equal-area projections (contours 1–2–4–6–8%; white dot: weighted average; great circle and black diamond: best fit girdle and its pole). Axial plane traces and foliations in the country rocks are from Fig. 2. Dashed lines in the pluton: facies boundaries (see Fig. 4a). Inset in the two parts of the figure (see Fig. 2 for details): Ly, Lyngdal granodiorite; HGG, high-grade gneiss.

(probable interference between emplacement of the pluton and regional deformation).

It is admitted that granitoid fabrics are acquired just before full crystallization, recording the last increments of displacement within the crystallizing magma (Paterson et al., 1998; Bouchez, 2000). Therefore, such fabrics may be called “magmatic”. In the KGC and SGC, most if not all of the evidence in favour of a syntectonic emplacement, especially fabric continuity across internal contacts and pluton margins, and widespread occurrence of intracrystalline deformation and recovery, strongly suggest that the “magmatic” fabric is largely controlled by the external, tectonic strain, despite the weak imprint of the latter. Consequently and except locally, the fabric attitude can hardly be interpreted in terms of magma flow and upwelling (Bouchez et al., 1990; Paterson et al., 1998; de Saint Blanquat et al., 2011).

In our plutons, the only portion where the fabric might have retain a certain “memory” of an igneous process concerns the second magmatic pulse in the SGC where locally, type 1 magmatic microstructures are observed in the Fa-facies. Nonetheless, the corresponding foliations and lineations are concordant with the neighbouring fabrics that display a tectonic imprint. Another particularity of the SGC is the discordance between fabrics of the two magmatic pulses located in the north of the pluton, likely reflecting a deflection of the fabric of the crystallizing Fa- and Opx-facies against the already crystallized, hence rigid Bt-facies. The concordance between a corridor of type 3 microstructures and the lineation pattern observed in the north and centre of the SGC concerns these deflected fabrics (Figs. 7b, 15b), suggesting strain localization associated with the deflection.

10.2. Emplacement during regional folding

Emplacement of the plutons during regional folding is supported by the geometrical relationships between their structure, as revealed by the AMS, and the folded structure of the country rocks. The KGC cuts across an overturned synform (Fig. 2), but appears in the hinge zone of the periclinal end of a probable F5 fold whose axial plane has a mean orientation of N176°E/76°E, with an axis orientated, in the outcrop area of the KGC, at N155°E/55°SSE (Petersen, 1973), very close (10°) to the mean magnetic lineation in the KGC (N160°E/48°SSE). Emplacement of the KGC within a fold core agrees with the dominantly prolate character of the magnetic fabric, particularly in the NW bulge of the pluton (Fig. 13c). Relationship between the SGC and the fold geometry of its wall rocks is more obscure. However, a NNW-SSE-striking, horizontal fold axis has been mapped close to the northern tip of the complex (Fig. 3; Jorde et al., 1995), and the lineations measured at the northern end of the SGC, in the Bt-facies, are subparallel to this fold axis (Fig. 15b). These observations support a synfolding emplacement.

Magnetic foliations organized around an axis parallel to the average magnetic lineation, as observed here, is a common feature in granitoids. In particular, this relationship has been described in synfolding plutons studied by Benn et al. (1997, 1998, 2001), Pignotta and Benn (1999), and Čečys and Benn (2007). In these case studies, either the foliation zone axis and the lineation are, in addition, parallel to the regional fold axes or we have a dominantly steeply-dipping foliation trending parallel to the axial surface trace of the regional folds. The magnetic foliations have been interpreted as folded flow-related foliations in the

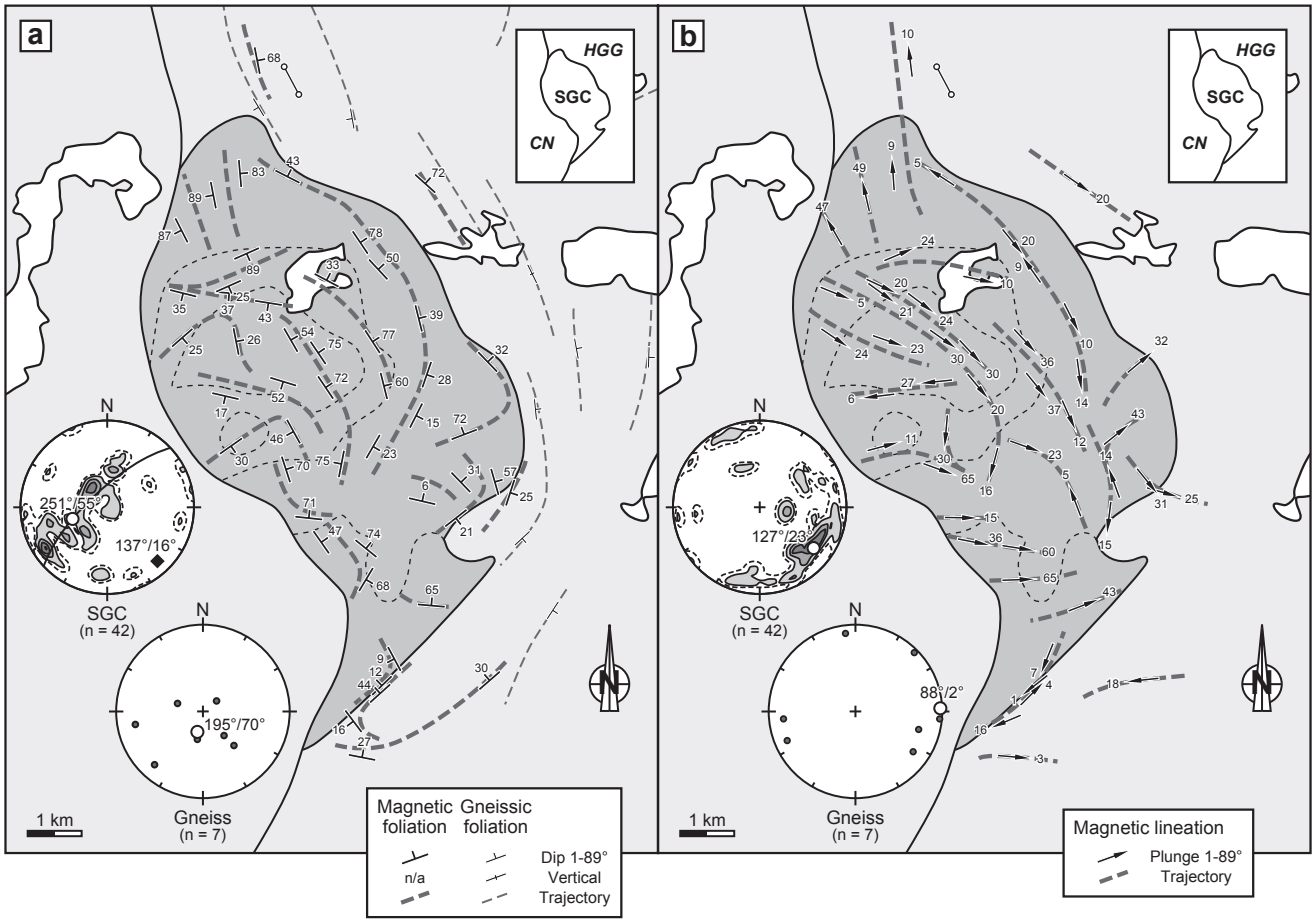

Fig. 15. Map of the magnetic (a) foliations and (b) lineations in the SGC, with lower hemisphere, equal-area projections (contours 1–2–4–6–8%; white dot: weighted average; great circle and black diamond: best fit girdle and its pole). The horizontal fold axis to the north of the SGC and the gneissic foliations are from Fig. 3. Dashed lines in the pluton: facies boundaries (see Fig. 4b). Inset in the two parts of the figure (see Fig. 3 for details): CN, Caledonian nappes; HGG, high-grade gneiss.

former case studies and as axial-planar fabrics in the latter. Our magnetic foliations would fit with the first interpretation for both the KGC and the SGC, except for the Bt-facies in the north of the SGC where the N-S-striking and steeply-dipping foliation is more akin to an axial-planar fabric.

We conclude that the KGC was emplaced during a folding event, probably equivalent to the F5 phase (Fig. 17a). Hence, its emplacement date (~937–935.5 Ma) provides an age for this regional-scale folding event. Concerning the SGC, there is no detailed structural study of its high-grade country rocks. However, we propose that it was also emplaced during the F5 folding phase, since its emplacement age is very close to that of the KGC. A model of synfolding emplacement is more difficult to put forward, given the uncertainties on the geometrical relationships between folds in the wall rocks and pluton structure. Therefore, the proposed model (Fig. 17b) focuses on the non-negligible repose time as given by the isotope chronology measurements.

11. Synfolding emplacement of late-Sveconorwegian granitoids in the Rogaland-Vest-Agder sector

The present model of synfolding emplacement complies with the one suggested by Bolle et al. (2003) as a conclusion of their AMS study of the Holum granite, a HBG pluton that crops out to the east of the KGC (Fig. 1b). A major argument was that the N-S-elongated Holum granite is in line with the southward end of a large-scale N-S-trending synform whose axis, in the southern part of the fold, is parallel to the magnetic lineations measured in the pluton. The large-scale synform was produced during the F5 phase (Bolle et al., 2003) and the emplacement age of the Holum granite, 957 ± 7 Ma (zircon U-Pb date; Bingen et al., 2006), dates this deformation event in the area. Combined with the present study, these data indicate that regional-scale folding in the RVA sector took place at 957–932.5 Ma and probably shortly after. Ductile deformation in this time interval, also constrained by Re-Os dating of molybdenite from small syndeformational deposits (Bingen et al., 2006), post-dates the 1.035–0.97 Ga peak of regional metamorphism (M1 phase). This event is here attributed to the F5 phase of Falkum (1998).

The synfolding model could apply to other late-Sveconorwegian plutons of the RVA sector, since many of them are aligned with the regional N-S-trending folded pattern. A conspicuous example is the voluminous Svöfjell HBG pluton (Fig. 1b) that was emplaced at 942 ± 10 Ma (U-Pb age; Vander Auwera et al., 2011). Some late-Sveconorwegian granitoids (Fig. 1b) representative of the "late-kinematic" intrusions of Starmer (1993) and Falkum (1998), such as the Homme granite (Falkum, 1976) and the Lygne complex (Bolle et al., 2003), are affected by *ca.* N-S-trending folds that may also be attributed to the F5 phase. It is worth noting that in addition to the F5 folds, some of these late-kinematic granitoids (*e.g.* the Lygne complex) are locally affected by *ca.* E-W folds attributed to F6. Actually, according to Starmer (1993), F5 and F6 folds are spatially associated at several places, displaying dome and basin patterns, and seem to have been almost coeval.

Using the present AMS data and those of Bolle et al. (2003), a mean magnetic lineation of N164°E/43°SSE can be calculated for the KGC, SGC and Holum granite, pointing to a *ca.* N-S and low-angle (< 45°) regional axis of stretching (*X* axis) in the south of the RVA sector at 957–932.5 Ma. Folding around this axis implies a *ca.* E-W and low-angle

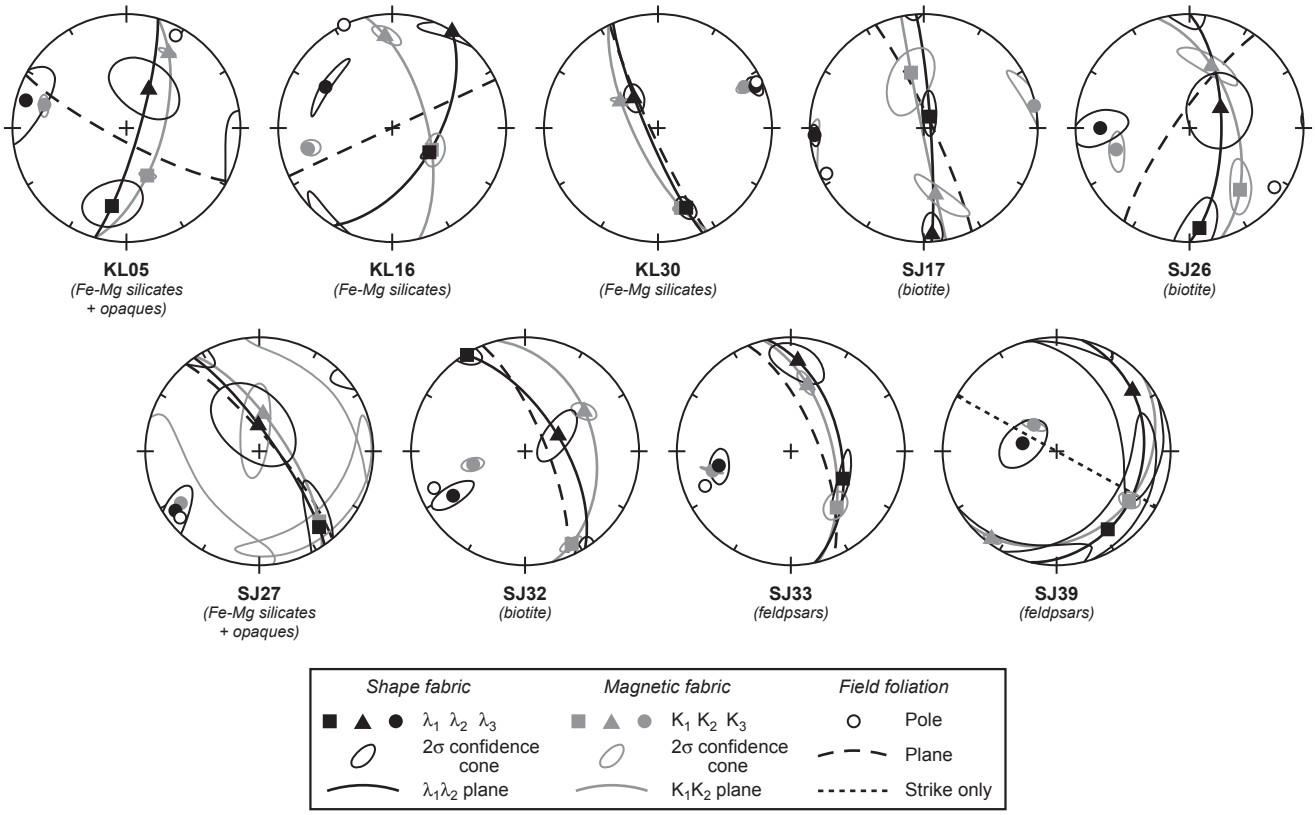

Fig. 16. Lower hemisphere, equal-area projections of the principal axes of the shape fabrics (λ_1, λ_2, λ_3) obtained from image analysis. The shape fabric is either that of mafic minerals or feldspars. Projections of the principal axes of the corresponding magnetic fabrics (K_1, K_2, K_3) and the mesoscopic-scale foliation are also shown, for comparison.

direction of shortening (*Z* axis). Such regional *X* and *Z* axes approximate the pattern of finite strain that would be produced either by a strike-slip deformation or by a strike-slip-dominated, homogeneous (*i.e.* not or weakly partitioned) transpression or transtension at low to moderate magnitude of strain (Fossen and Tikoff, 1998). We think this observation is significant for better constraining the tectonic context of the late-Sveconorwegian magmatism in the RVA sector, traditionally considered as being extensional (Bingen et al., 2006, 2008b; Slagstad et al., 2013). However, its discussion is outside the scope of this study. We simply note that the strike-slip explanation is probably irrelevant and that transpression is a viable alternative to extension or transtension since this regime can also promote the emplacement of granitoids, as well as the exhumation of deep crustal rocks causing extensional movements (Ferré et al., 2002; Corsini and Rolland, 2009).

12. Conclusions

Precise U-Pb dating of zircons from various facies of the KGC and SGC imply penecontemporaneous emplacement of these two composite granitic complexes, respectively at ~937–935.5 Ma and ~935.5–932.5 Ma. These dates fall in the interval of U-Pb ages previously found by several authors for the HBG and AMC suites. It is thus confirmed that the KGC and SGC are two representatives of the late-Sveconorwegian magmatism, including the Bt-facies of the SGC previously considered as belonging to the 1.06–1.02 Ga Sirdal magmatic belt. The U-Pb geochronological data further confirm that the Fa- and Opx-facies are younger than the Bt-facies in the SGC, with a repose time of ~3.2 Ma. Crosscutting relationships locally observed between magnetic fabrics of the two magmatic pulses agree with such a marked time gap. Both the U-Pb and AMS data do not reveal significant repose times in the KGC, hence the separate magma batches were emplaced more-or-less coevally.

The present study demonstrates that the KGC and the SGC were emplaced in a tectonic strain field, their fabric being largely controlled by the deformation of the wall-rocks, rather than by magma dynamics. Concordance of the magnetic fabrics with the folded structure of the high-grade country rocks allows proposing a synfolding emplacement of the complexes, coeval with the last stage of Sveconorwegian contraction recorded in the area, namely the F5(-F6) folding event. This model, that agrees with the emplacement scenario previously suggested for the Holum granite, could probably apply to other late-Sveconorwegian plutons of the RVA sector. Emplacement ages of the complexes and that published elsewhere for the Holum granite bracket the age of F5(-F6) between 957 and 932.5 Ma, attesting that regional-scale folding was still active in the RVA sector up to *ca.* 40 Ma after the 1.035–0.97 Ga peak of regional metamorphism (M1 phase).

Acknowledgements

J.R. Wilson is warmly thanked for the Danish to English translation of the paper by Petersen (1973). We also express our gratitude to B. Bingen who assisted us in the interpretation of the U-Pb geochronological data. N. Coint is thanked for the high definition map she sent, which helped us to update the geology of the country rocks of the Sjelset granitic complex. Field work was partly funded by the F.N.R.S. (National Fund for Scientific Research, Belgium). Technical assistance was received from J.-P. Cullus. We thank J.-L. Bouchez and an anonymous reviewer for their insightful and constructive reviews that significantly aided to improve the manuscript. Journal editor R.R. Parrish is thanked for his comments and handling the manuscript.

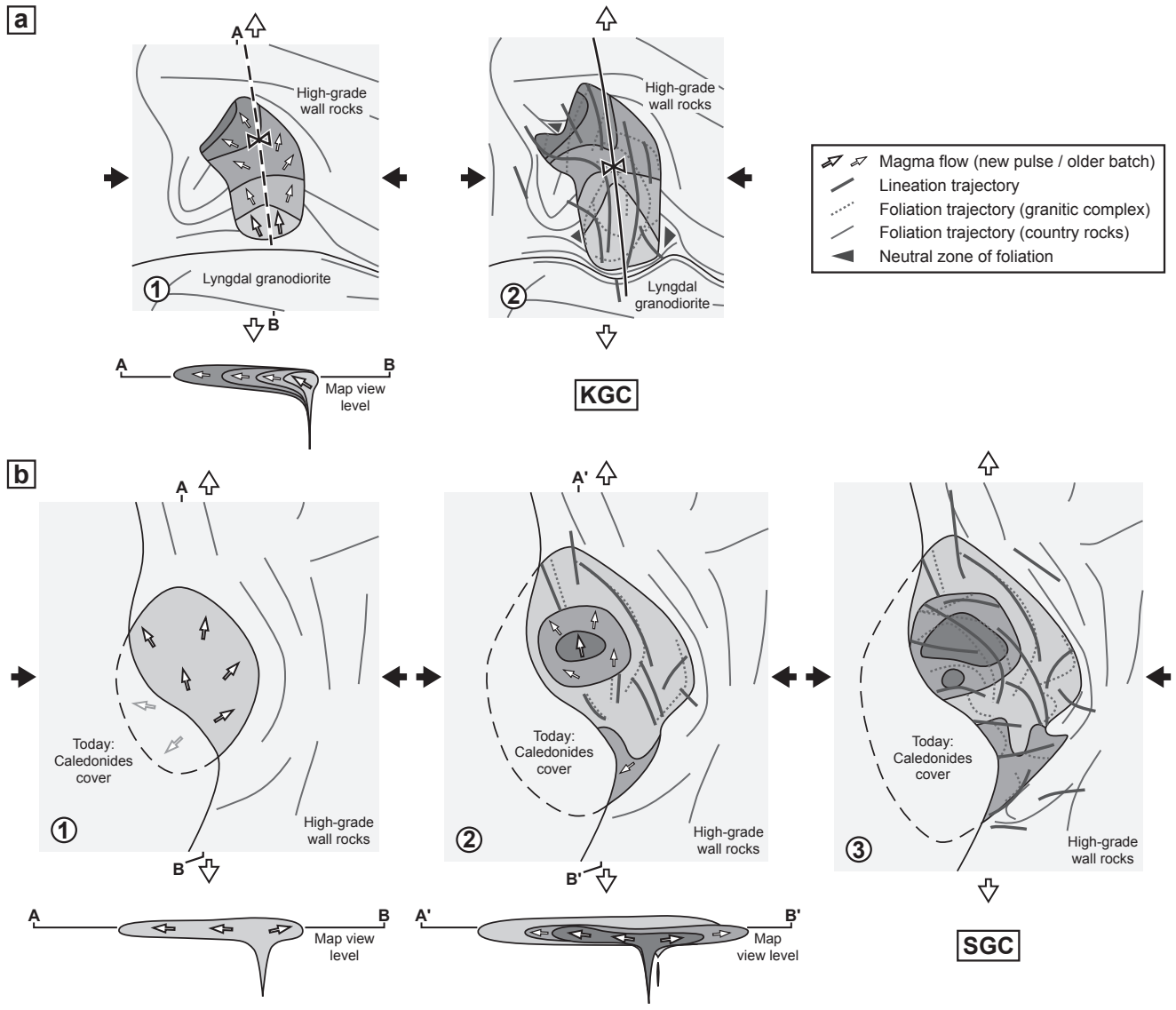

Fig. 17. Models of emplacement and deformation. (a) For the KGC: 1, emplacement of almost coeval magma pulses within the periclinal end of a growing F5 synform (it is considered that the emplacement was progressing northwards along the steepening southward plunge of the fold hinge; the focus is on the injection of the Bt facies, the most evolved lithology, supposed to be the youngest magmatic pulse); 2, final structure of the pluton, influenced be the regional tectonics. (b) For the SGC: 1, emplacement of the Bt-facies, forming a proto-pluton, the feeding zone being hypothetically located below the southern part of the growing magmatic body; 2, penecontemporaneous emplacement of the Fa and Opx-facies, the latter being supposed to be slightly younger than the former, across the Bt-facies pulse; 3, final structure of the SGC, influenced by the regional tectonics and the internal rheological contrasts responsible for fabric deflection against the rigid northern end. A N-S direction of stretching (*X* axis; white arrows) and an E-W direction of shortening (*Z* axis; black arrows) are taken into account in both models (see text).

Appendices A. Supplementary data

Supplementary data associated with this article can be found, in the online version, at http://dx.doi.org/10.1016/j.precamres.2017.12.012.

References

Andersen, T., Andresen, A., Sylvester, A.G., 2001. Nature and distribution of deep crustal reservoirs in the southwestern part of the Baltic Shield: evidence from Nd, Sr and Pb isotope data on late Sveconorwegian granites. J. Geol. Soc., London 158, 253–267.

Barboni, M., Schoene, B., Ovtcharova, M., Bussy, F., Schaltegger, U., Gerdes, A., 2013. Timing of incremental pluton construction and magmatic activity in a back-arc setting revealed by ID-TIMS U/Pb and Hf isotopes on complex zircon grains. Chem. Geol. 340, 76–93.

Benn, K., Horne, R.J., Kontak, D.J., Pignotta, G.S., Evans, N.G., 1997. Syn-Acadian emplacement model for the South Mountain batholith, Meguma Terrane, Nova Scotia: magnetic fabric and structural analyses. Geol. Soc. Am. Bull. 109, 1279–1293.

Benn, K., Ham, N.M., Pignotta, G.S., Bleeker, W., 1998. Emplacement and deformation of granites during transpression: magnetic fabrics of the Archean Sparrow pluton, Slave Province, Canada. J. Struct. Geol. 20, 1247–1259.

Benn, K., Paterson, S.R., Lund, S.P., Pignotta, G.S., Kruse, S., 2001. Magmatic fabrics in batholiths as markers of regional strains and plate kinematics: example of the Cretaceous Mt. Stuart batholith. Phys. Chem. Earth (Part A) 26, 343–354.

Bingen, B., Demaiffe, D., van Breemen, O., 1996. Rb-Sr isotopic signature of augen gneiss suites in the Sveconorwegian Province of SW Norway. In: Demaiffe, D. (Ed.), Petrology and Geochemistry of Magmatic Suites of Rocks in the Continental and Oceanic Crusts. U.L.B.-M.R.A.C, Bruxelles, pp. 161–174.

Bingen, B., Davis, W.J., Hamilton, M.A., Engvik, A.K., Stein, H.J., Skår, Ø., Nordgulen, Ø., 2008a. Geochronology of high-grade metamorphism in the Sveconorwegian belt, S. Norway: U-Pb, Th-Pb and Re-Os data. Norw. J. Geol. 88, 13–42.

Bingen, B., Nordgulen, Ø., Viola, G., 2008b. A four-phase model for the Sveconorwegian orogeny, SW Scandinavia. Norw. J. Geol. 88, 43–72.

Bingen, B., Skår, Ø., Marker, M., Sigmond, E.M.O., Nordgulen, Ø., Ragnhildstveit, J., Mansfeld, J., Tucker, R.D., Liégeois, J.P., 2005. Timing of continental building in the Sveconorwegian orogen, SW Scandinavia. Norw. J. Geol. 85, 87–116.

Bingen, B., Stein, H.J., Bogaerts, M., Bolle, O., Mansfeld, J., 2006. Molybdenite Re-Os dating constrains gravitational collapse of the Sveconorwegian orogen, SW Scandinavia. Lithos 87, 328–346.

Bingen, B., van Breemen, O., 1998. Tectonic regimes and terrane boundaries in the high-grade Sveconorwegian belt of SW Norway, inferred from U-Pb zircon geochronology and geochemical signature of augen gneiss suites. J. Geol. Soc., London 155, 143–154.

Bogaerts, M., Scaillet, B., Liégeois, J.P., Vander Auwera, J., 2003. Petrology and

geochemistry of the Lyngdal granodiorite (Southern Norway) and the role of fractional crystallisation in the genesis of Proterozoic ferro-potassic A-type granites. Precambr. Res. 124, 149–184.
Bogdanova, S.V., Bingen, B., Gorbatschev, R., Kheraskova, T.N., Kozlov, V.I., Puchkov, V.N., Volozh, Y.A., 2008. The East European Craton (Baltica) before and during the assembly of Rodinia. Precambr. Res. 160, 23–45.
Bolle, O., Diot, H., Trindade, R.I.F., 2003. Magnetic fabrics in the Holum granite (Vest-Agder, southermost Norway): implications for the late evolution of the Sveconorwegian (Grenvillian) orogen of SW Scandinavia. Precambr. Res. 121, 221–249.
Bolle, O., Diot, H., Liégeois, J.P., Vander Auwera, J., 2010. The Farsund intrusion (SW Norway): a marker of late-Sveconorwegian (Grenvillian) tectonism emplaced along a newly defined major shear zone. J. Struct. Geol. 32, 1500–1518.
Bouchez, J.L., 2000. Anisotropie de susceptibilité magnétique et fabrique des granites. Comptes Rendus de l'Académie des Sciences, Paris, Sciences de la Terre et des Planètes 330, 1–14.
Bouchez, J.L., Gleizes, G., Djouadi, T., Rochette, P., 1990. Microstructure and magnetic susceptibility applied to emplacement kinematics of granites: the example of the Foix pluton (French Pyrenees). Tectonophysics 184, 157–171.
Čečys, A., Benn, K., 2007. Emplacement and deformation of the *ca.* 1.45 Ga Karlshamn granitoid pluton, southeastern Sweden, during ENE-WSW Danopolonian shortening. Int. J. Earth Sci. 96, 397–414.
Clark, D.A., 1997. Magnetic petrophysics and magnetic mineralogy: aids to geological interpretation of magnetic surveys. J. Aust. Geol. Geophys. 17, 83–103.
Coint, N., Slagstad, T., Roberts, N.M.W., Marker, M., Røhr, T., Sørensen, B.E., 2015. The Late Mesoproterozoic Sirdal Magmatic Belt, SW Norway: relationships between magmatism and metamorphism and implications for Sveconorwegian orogenesis. Precambr. Res. 265, 57–77.
Corsini, M., Rolland, Y., 2009. Late evolution of the southern European Variscan belt: exhumation of the lower crust in a context of oblique convergence. C.R. Geosci. 341, 214–223.
D'Lemos, R.S., Brown, M., Strachan, R.A., 1992. Granite magma generation, ascent and emplacement within a transpressional orogen. J. Geol. Soc., London 149, 487–490.
Drüppel, K., Elsäßer, L., Brandt, S., Gerdes, A., 2013. Sveconorwegian mid-crustal ultrahigh-temperature metamorphism in Rogaland, Norway: U-Pb LA-ICP-MS geochronology and pseudosections of sapphirine granulites and associated paragneisses. J. Petrol. 54, 305–350.
Duchesne, J.C., 1972. Iron-titanium oxide minerals in the Bjerkrem-Sogndal massif, south-western Norway. J. Petrol. 13, 57–81.
Duchesne, J.C. (Ed.), 2001. The Rogaland intrusive massifs: an excursion guide. Norges geologiske undersøkelse Report 2001.029, 139 p.
Duchesne, J.C., Maquil, R., Demaiffe, D., 1985. The Rogaland anorthosites: facts and speculations. In: Tobi, A.C., Touret, J.L.R. (Eds.), The Deep Proterozoic Crust in the North Atlantic Provinces. Reidel, Dordrecht, pp. 449–476.
Dunlop, D.J., Özdemir, Ö., 2009. Magnetizations in rocks and minerals. In: Kono, M. (Ed.), Treatise of Geophysics. Geomagnetism, vol. 5. Elsevier, Amsterdam, pp. 277–336.
Eliasson, T., Ahlin, S., Petersson, J., 2003. Emplacement mechanism and thermobarometry of the Sveconorwegian Bohus granite, SW Sweden. Geologiska Föreningens i Stockholm Förhandlingar 125, 113–130.
Falkum, T., 1976. The structural geology of the Precambrian Homme granite and the enveloping banded gneisses in the Flekkefjord area, Vest-Agder, Southern Norway. Norges geologiske undersøkelse 324, 79–101.
Falkum, T., 1982. Geologisk Kart Over Norge, Berggrunnskart Mandal – 1:250000. Norges geologiske undersøkelse, Trondheim.
Falkum, T., 1998. The Sveconorwegian magmatic and tectonometamorphic evolution of the high-grade Proterozoic Flekkefjord complex, South Norway. Norges geologiske undersøkelse Bulletin 434, 5–33.
Falkum, T., Petersen, J.S., 1974. A three-fold division of the 'farsundite' plutonic complex at Farsund, southern Norway. Nor. Geol. Tidsskr. 54, 361–366.
Ferré, E.C., Gébelin, A., Till, J.L., Sassier, C., Burmeister, K.C., 2014. Deformation and magnetic fabrics in ductile shear zones: a review. Tectonophysics 629, 179–188.
Ferré, E., Gleizes, G., Caby, R., 2002. Obliquely convergent tectonics and granite emplacement in the Trans-Saharan belt of Eastern Nigeria: a synthesis. Precambr. Res. 114, 199–219.
Fossen, H., Tikoff, B., 1998. Extended models of transpression and transtension, and application to tectonic settings. In: Holdsworth, R.E., Strachan, R.A., Dewey, J.F. (Eds.), Continental transpressional and transtensional tectonics, Geological Society, London, Special Publications 135, pp. 15–33.
Gleizes, G., Leblanc, D., Santana, V., Olivier, P., Bouchez, J.L., 1998. Sigmoidal structures featuring dextral shear during emplacement of the Hercynian granite complex of Cauterets-Panticosa (Pyrenees). J. Struct. Geol. 20, 1229–1245.
Gleizes, G., Nédélec, A., Bouchez, J.L., Autran, A., Rochette, P., 1993. Magnetic susceptibility of the Mont-Louis Andorra ilmenite-type granite (Pyrenees): a new tool for the petrographic characterization and regional mapping of zoned granite plutons. J. Geophys. Res. 98 (B3), 4317–4331.
Henry, B., Liégeois, J.P., Nouar, O., Derder, M.E.M., Bayou, B., Bruguier, O., Ouabadi, A., Belhai, D., Amenna, M., Hemmi, A., Ayache, M., 2009. Repeated granitoid intrusions during the Neoproterozoic along the western boundary of the Saharan metacraton, Eastern Hoggar, Tuareg shield, Algeria: an AMS and U-Pb zircon age study. Tectonophysics 474, 417–434.
Hoskin, P.W.O., Schaltegger, U., 2003. The composition of zircon and igneous and metamorphic petrogenesis. Rev. Mineral. Geochem. 53, 27–62.
Hrouda, F., 1994. A technique for the measurement of thermal changes of magnetic susceptibility of weakly magnetic rocks by the CS-2 apparatus and KLY-2 Kappabridge. Geophys. J. Int. 118, 604–612.
Hutton, D.H.W., 1988. Granite emplacement mechanisms and tectonic controls: inferences from deformation studies. Trans. R. Soc. Edinburgh, Earth Sci. 79, 245–255.
Jacamon, F., Larsen, R.B., 2009. Trace element evolution of quartz in the charnockitic Kleivan granite, SW-Norway: the Ge/Ti ratio of quartz as an index of igneous differentiation. Lithos 107, 281–291.
Jelínek, V., 1981. Characterization of magnetic fabric of rocks. Tectonophysics 79, T63–T67.
Jorde, K., Sigmond, E.M.O., Thorsnes, T., 1995. Geologisk Kart Over Norge, Berggrunnskart Stavanger – 1:250000. Norges geologiske undersøkelse, Trondheim.
Li, Z.X., Bogdanova, S.V., Collins, A.S., Davidson, A., De Waele, B., Ernst, R.E., Fitzsimons, I.C.W., Fuck, R.A., Gladkochub, D.P., Jacobs, J., Karlstrom, K.E., Lu, S., Natapov, L.M., Pease, V., Pisarevsky, S.A., Thrane, K., Vernikovsky, V., 2008. Assembly, configuration, and break-up history of Rodinia: a synthesis. Precambr. Res. 160, 179–210.
Maijer, C., 1987. The metamorphic envelope of the Rogaland intrusive complex. In: Maijer, C., Padget, P. (Eds.), The geology of southernmost Norway: an excursion guide. Norges geologiske undersøkelse, Special Publication 1, pp. 68–73.
Maijer, C., Verschure, R.H., Visser, D., 1994. Strontium isotope study of two supposed satellite massifs of the Egersund Anorthosite Complex: the Sjelset Igneous Complex and the Undheim Leuconorite. Nor. Geol. Tidsskr. 74, 58–69.
Mainprice, D., Bouchez, J.L., Blumenfeld, P., Tubia, J.M., 1986. Dominant c-slip in naturally deformed quartz: implications for dramatic plastic softening at high temperature. Geology 14, 819–822.
Marker, M., Schiellerup, H., Meyer, G.B., Robins, B., Bolle, O., 2003. Geological map of the Rogaland anorthosite province – Scale 1:75000. In: Duchesne, J.C., Korneliussen, A. (Eds.), Ilmenite deposits and their geological environment. With special reference to the Rogaland anorthosite province. Norges geologiske undersøkelse, Special Publication 9, Plate 1.
Michot, P., 1960. La géologie de la catazone: le problème des anorthosites, la palingenèse basique et la tectonique catazonale dans le Rogaland méridional (Norvège méridionale). Norges geologiske undersøkelse 212g, pp. 1–54.
Passchier, C.W., Trouw, R.A.J., 2005. Microtectonics, second ed. Springer-Verlag, Berlin, Heidelberg xvi + 366 p.
Paterson, S.R., Fowler Jr., T.K., Schmidt, K.L., Yoshinobu, A.S., Yuan, E.S., Miller, R.B., 1998. Interpreting magmatic fabric patterns in plutons. Lithos 44, 53–82.
Petersen, J.S., 1973. Geometrisk analyse af et polyfasefoldet grundfjeldskompleks. Dansk geologisk Forening, Årsskrift for 1973, 71–81.
Petersen, J.S., 1977. The migmatite complex near Lyngdal, southern Norway, and related granulite metamorphism. Nor. Geol. Tidsskr. 57, 65–83.
Petersen, J.S., 1980. The zoned Kleivan granite – an end member of the anorthosite suite in southwest Norway. Lithos 13, 79–95.
Petersen, J.S., Pedersen, S., 1978. Strontium-isotope study of the Kleivan granite, southern Norway. Nor. Geol. Tidsskr. 58, 97–102.
Petrovský, E., Kapička, A., 2006. On determination of the Curie point from thermomagnetic curves. J. Geophys. Res. 111, B12S27.
Pignotta, G.S., Benn, K., 1999. Magnetic fabric of the Barrington Passage pluton, Meguma Terrane, Nova Scotia: a two-stage fabric history of syntectonic emplacement. Tectonophysics 307, 75–92.
Robinson, P., Fabian, K., McEnroe, S.A., Heidelbach, F., 2013. Influence of lattice-preferred orientation with respect to magnetizing field on intensity of remanent magnetization in polycrystalline hemo-ilmenite. Geophys. J. Int. 192, 514–536.
Rochette, P., 1987. Magnetic susceptibility of the rock matrix related to magnetic fabric studies. J. Struct. Geol. 9, 1015–1020.
Román-Berdiel, T., Casas, A.M., Oliva-Urcia, B., Pueyo, E.L., Rillo, C., 2004. The main Variscan deformation event in the Pyrenees: new data from the structural study of the Bielsa granite. J. Struct. Geol. 26, 659–677.
de Saint Blanquat, M., Horsman, E., Habert, G., Morgan, S., Vanderhaeghe, O., Law, R., Tikoff, B., 2011. Multiscale magmatic cyclicity, duration of pluton construction, and the paradoxical relationship between tectonism and plutonism in continental arcs. Tectonophysics 500, 20–33.
de Saint Blanquat, M., Tikoff, B., 1997. Development of magmatic to solid-state fabrics during syntectonic emplacement of the Mono Creek Granite, Sierra Nevada batholith. In: Bouchez, J.L., Hutton, D.H.W., Stephens, W.E. (Eds.), Granite: From Segregation of Melt to Emplacement Fabrics. Kluwer, Dordrecht, pp. 231–252.
Sauer, S., 2011. A Lu-Hf isotope study of zircons from high-alumina orthopyroxene megacrysts from the Neoproterozoic Rogaland Anorthosite Province, SW Norway: A window to the Sveconorwegian lower crust. Unpublished MSc Thesis. University of Bremen 87 p.
Sauter, P.C.C., Hermans, G.A.E.M., Jansen, J.B.H., Maijer, C., Spits, P., Wegelin, A., 1983. Polyphase Caledonian metamorphism in the Precambrian basement of Rogaland/Vest-Agder, SW Norway. Norges geologiske undersøkelse 380, 7–22.
Schärer, U., Wilmart, E., Duchesne, J.C., 1996. The short duration and anorogenic character of anorthosite magmatism: U-Pb dating of the Rogaland complex, Norway. Earth Planet. Sci. Lett. 139, 335–350.
Schaltegger, U., Brack, P., Ovtcharova, M., Peytcheva, I., Schoene, B., Stracke, A., Marocchi, M., Bargossi, G.M., 2009. Zircon and titanite recording 1.5 million years of magma accretion, crystallization and initial cooling in a composite pluton (southern Adamello batholith, northern Italy). Earth Planet. Sci. Lett. 286, 208–218.
Sigmond, E.M.O., Gustavson, M., Roberts, D., 1984. Berggrunnskart Over Norge – 1:1000000. Norges geologiske undersøkelse, Trondheim.
Slagstad, T., Roberts, N.M.W., Marker, M., Røhr, T.S., Schiellerup, H., 2013. A non-collisional, accretionary Sveconorwegian orogen. Terra Nova 25, 30–37.
Starmer, I.C., 1993. The Sveconorwegian Orogeny in southern Norway, relative to deep crustal structures and events in the North Atlantic Proterozoic Supercontinent. Nor. Geol. Tidsskr. 73, 109–132.
Stipp, M., Stünitz, H., Heilbronner, R., Schmid, S.M., 2002. The eastern Tonale fault zone:

a 'natural laboratory' for crystal plastic deformation of quartz over a temperature range from 250 to 700 °C. J. Struct. Geol. 24, 1861–1884.
Tobi, A.C., Hermans, G.A.E.M., Maijer, C., Jansen, J.B.H., 1985. Metamorphic zoning in the high-grade Proterozoic of Rogaland-Vest Agder, SW Norway. In: Tobi, A.C., Touret, J.L.R. (Eds.), The Deep Proterozoic Crust in the North Atlantic Provinces. Reidel, Dordrecht, pp. 477–497.
Vander Auwera, J., Bogaerts, M., Bolle, O., Longhi, J., 2008. Genesis of intermediate igneous rocks at the end of the Sveconorwegian (Grenvillian) orogeny (S Norway) and their contribution to intracrustal differentiation. Contrib. Miner. Petrol. 156, 721–743.
Vander Auwera, J., Bogaerts, M., Liégeois, J.P., Demaiffe, D., Wilmart, E., Bolle, O., Duchesne, J.C., 2003. Derivation of the 1.0-0.9 Ga ferro-potassic A-type granitoids of southern Norway by extreme differentiation from basic magmas. Precambr. Res. 124, 107–148.
Vander Auwera, J., Bolle, O., Bingen, B., Liégeois, J.P., Bogaerts, M., Duchesne, J.C., De Waele, B., Longhi, J., 2011. Sveconorwegian massif-type anorthosites and related granitoids result from post-collisional melting of a continental arc root. Earth Sci. Rev. 107, 375–397.
Vander Auwera, J., Bolle, O., Dupont, A., Pin, C., Paquette, J.L., Charlier, B., Duchesne, J.C., Mattielli, N., Bogaerts, M., 2014. Source-derived heterogeneities in the composite (charnockite-granite) ferroan Farsund intrusion (SW Norway). Precambr. Res. 251, 141–163.
Vernon, R.H., 2000. Review of microstructural evidence of magmatic and solid-state flow. Electron. Geosci. 5 (2), 1–23.
Verschure, R.H., Andriessen, P.A.M., Boelrijk, N.A.I.M., Hebeda, E.H., Maijer, C., Priem, H.N.A., Verdurmen, E.A.T., 1980. On the thermal stability of Rb-Sr and K-Ar biotite systems: evidence from coexisting sveconorwegian (ca. 870 Ma) and Caledonian (ca. 400 Ma) biotites in SW Norway. Contrib. Miner. Petrol. 74, 245–252.